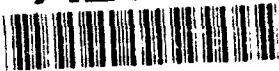


AD-A269 882



IDENTIFICATION PAGE

Form Approved
OMB No 0704-0188

Estimated to save space in publication, this page contains information that is not required for the full text of the report. This information is available in the full text of the report and is not to be used for the purpose of this document. The Office of Management and Budget Paperwork Reduction Project (0704-0188) is responsible for this information.

REPORT DATE

3. REPORT TYPE AND DATES COVERED

ANNUAL 01 Aug 92 TO 31 Jul 93

4. TITLE AND SUBTITLE

LITHOSPHERIC PROFILES IN THE SOUTHWESTERN U.S. USING
NEVADA TEST SITE SOURCES

5. FUNDING NUMBERS

F49620-92-J-0438

61102F

2309

AS

6. AUTHOR(S)

Dr G. Randy Keller

7. PERFORMING ORGANIZATION NAME(S) AND ADDRESS(ES)

Dept of Geological Sciences
Univ of Texas, El Paso
500 West University
El Paso, TX 799688. PERFORMING ORGANIZATION
REPORT NUMBER

AFOSR-78

9. SPONSORING / MONITORING AGENCY NAME(S) AND ADDRESS(ES)

AFOSR/NL
110 Duncan Avenue, Suite B115
Bolling AFB DC 20332-0001
Dr Stanley K. Dickinson10. SPONSORING / MONITORING
AGENCY REPORT NUMBER

11. SUPPLEMENTARY NOTES

DTIC
ELECTE
SEP 28 1993
S A D

12a. DISTRIBUTION / AVAILABILITY STATEMENT

Approved for public release;
distribution unlimited

12b. DISTRIBUTION CODE

13. ABSTRACT (Maximum 200 words) The objective of this grant is to conduct a variety of seismic investigations in the southwestern U.S. and to use the results to determine lithospheric structure and seismic wave propagation in the region. The 'Minor Uncle' explosion at the White Sands Missile Range (WSMR) was recorded in June, 1993 and the resultant data has been interpreted in the effort to establish a lithospheric transect between the Nevada Test Site (NTS) and the WSMR. Data sets have been obtained for the tomographic study of the Mojave desert area and the initial modeling has begun to form the basis for tomographic inversions. Valuable experience with tomographic techniques has been gained by applying them to Pg phase data from the 1989 PACE (Pacific to Arizona Crustal Experiment) experience. An excellent picture of upper crustal structure in the PACE area is emerging from combining the tomographic results, Pg phase inversions, and analysis of gravity anomalies. Analysis of the eastern part of the NTS-WSMR profile reveals that the deep lithospheric effects of the Rio Grande rift are more pronounced than previously predicted and the effects extend about 100 km beyond the physiographic boundaries of the rift. An important framework has been established for the upcoming refraction experiment in the Sierra Nevada region.

14. SUBJECT TERMS

93-22348



15. NUMBER OF PAGES

16. PRICE CODE

17. SECURITY CLASSIFICATION
OF REPORT

(U)

OF THIS PAGE

(U)

18. SECURITY CLASSIFICATION
OF ABSTRACT

(U)

20. LIMITATION OF ABSTRACT

(UL)

**University of Texas at El Paso
Department of Geological Sciences
Annual Technical Report
Grant Number F49620-J-0438**

**Lithospheric Profiles in the Southwestern U.S. Using Nevada Test Site Sources
Principal Investigators: G. Randy Keller, Diane I. Doser, Kate C. Miller**

SUMMARY

The objectives of this project are to conduct a variety of seismic studies in the southwestern U.S. and to use the results to investigate lithospheric structure and seismic wave propagation in the area. In this first year of this project, good progress has occurred on all fronts. We successfully re-recorded the Minor Uncle explosion on the White Sands Missile Range (WSMR) in June of 1993. These data have already been played back, edited, merged, and plotted in record section form. A preliminary interpretation is also complete. This is a major step in our ongoing effort to work on a lithospheric transect extending between NTS and WSMR.

We have also made good progress on the tomographic study of the Mojave desert area. Data from the Cal Tech and U.S. Geological Survey networks in the region have been obtained. We have implemented software for tomographic analysis and are close to making initial runs on the combined data set. We gained valuable experience with tomographic techniques by applying them to Pg phase data from the 1989 PACE experiment. The analysis of the large PACE data set is nearly complete. Inverse methods were applied to the Pg phase from the portion of the data set which lies along the NTS-WSMR transect which, when combined with the tomographic results and analysis of gravity anomalies, provides an excellent picture on upper crustal structure in the area. Inversion of wide-angle reflections from deeper horizons in the crust and upper mantle is almost complete and initial results provide an explanation for some of the apparently contradictory previous results.

DTIC QUALITY INSPECTED 3

A-1
16 SEP 1993

The analysis of the eastern portion of the NTS-WSMR profile was completed as the subject of an M.S. thesis. Seismic data were recorded to offsets of 1250 km. These data reveal that the deep lithospheric effects of the Rio Grande rift are more pronounced than predicted by regional models of western U. S. seismic structure. In addition, the eastern extent of these effects extend beyond the physiographic boundaries of the rift by about 100 km.

Our receiver function studies are continuing with our analysis of the Lajitas station in west Texas being almost complete. The regional analysis of surface wave dispersion is also nearly complete.

The unexpected cessation of testing at NTS has caused some reorganization of our seismic profiling efforts. The conventional explosion of the Non-Proliferation Experiment at the NTS, originally planned for early 1993, has provided a very appropriate alternative. This explosion was delayed until September, 1993 because of safety concerns. This delay turned out to be very fortuitous because it provided an opportunity to interface with a major seismic experiment targeting the Sierra Nevada Mountains. By cooperating with this experiment, we will be able to record a long profile extending westward from NTS across this mountain range and significantly add to the overall success of this large cooperative effort. A much improved picture of earth structure around NTS will result, and the effects of the deep structure of mountain ranges on seismic waves is a major concern in efforts to monitor seismic events in many areas around the world. This effort represents only a minor change in our planned activities in that we will be recording along a profile extending westward from NTS instead of southeastward. We plan to record along the southeastward profile in the second year of the project

Detailed descriptions of our main results to date follow this overview of our activities

PUBLICATIONS

Adams, D.C. and G.R. Keller, 1993, Crustal Structure and Basin Geometry in South-central New Mexico: Geological Society of America, Rio Grande Rift Memoir, in press.

Durrani, B., G.R. Keller, and D. I. Doser, 1993, Upper Crustal Structure of the Colorado Plateau Determined from Inversion and Tomography of Pg Phases: Journal of Geophysical Research, in preparation.

Miller, K.C. and W.D. Mooney, 1993, Crustal Structure of the Southern Foothills Metamorphic Belt, Sierra Nevada, California, from Seismic Data: Journal of Geophysical Research, in revision.

Schneider, R.V. and G.R. Keller, 1993, Crustal Structure of the Western Margin of the Rio Grande Rift and Mogollon-Datil Volcanic Field, Southwestern New Mexico and Southern Arizona: Geological Society of America, Rio Grande Rift Memoir, in press.

PERSONNEL

The Principal Investigators on this project are G. Randy Keller, Diane I. Dose, and Kate C. Miller. In addition, the following students have been involved to a significant extent:

Donald Roberts, Carlos Montana, Donald Adams, Bashir Durrani, Raed Aldouri, Julia Whitelaw, and Alejandro Duran. Donald Roberts completed his M. S. thesis in May, 1993 and Bashir Durrani and Raed Aldouri are nearing completion of their Ph.D. theses. Mr. Durrani's defense is scheduled for September 7.

Roberts, Donald G., 1993, A Long Offset Seismic Profile Across the Rio Grande Rift and Its Transi-

tion Zones in Central New Mexico: M. S. Thesis, 64p.

Detailed Descriptions of Specific Projects

Tomographic and Surface Wave Studies of the Mojave Region

We have compiled two important data sets for studies of the crustal structure of the Mojave Block and adjacent regions. P- and S-wave arrival times for earthquakes and nuclear tests within a region extending from 114°W to 118.5°W and the U.S.-Mexico border to 38°N (Figure 1) recorded at seismograph stations operated by Caltech, the U.S.G.S. and the University Nevada-Reno have been collected for a tomographic study of the region's crustal structure. We are currently using available geologic and geophysical information to construct a series of block models that will be used as starting models for the tomographic inversions. A diagram illustrating the seismic ray coverage (and hence the anticipated resolution of velocity structure within the region) for a selected group of events is shown in Figure 2. Ms. Julie Whitelaw is conducting this study as part of her dissertation research under the direction of Dr. Doser.

A second data set we have compiled is surface wave information from teleseisms located along great circle paths between the seismograph stations shown in Figure 3. These data will be used to determine the shear wave structure across the study area. Of particular interest is the deep regional shear velocity information obtained from surface waves with periods > 50 sec. Drs. Charles Ammon (Univ. Calif.-Santa Cruz) and Howard Patton (Lawrence Livermore Lab.) are currently conducting a study of surface waves from regional earthquakes (periods < 50 sec) throughout the western United States. We hope to integrate our results from the teleseismic studies with their ongoing work to produce a detailed model of the shear velocity structure from the upper crust to upper mantle. Some of the data for our study are available in digital format, however seismograms from stations JAS, ISA, GSC, TUC, and ALQ (analog station prior to ANMO) must be copied from microfiche and then

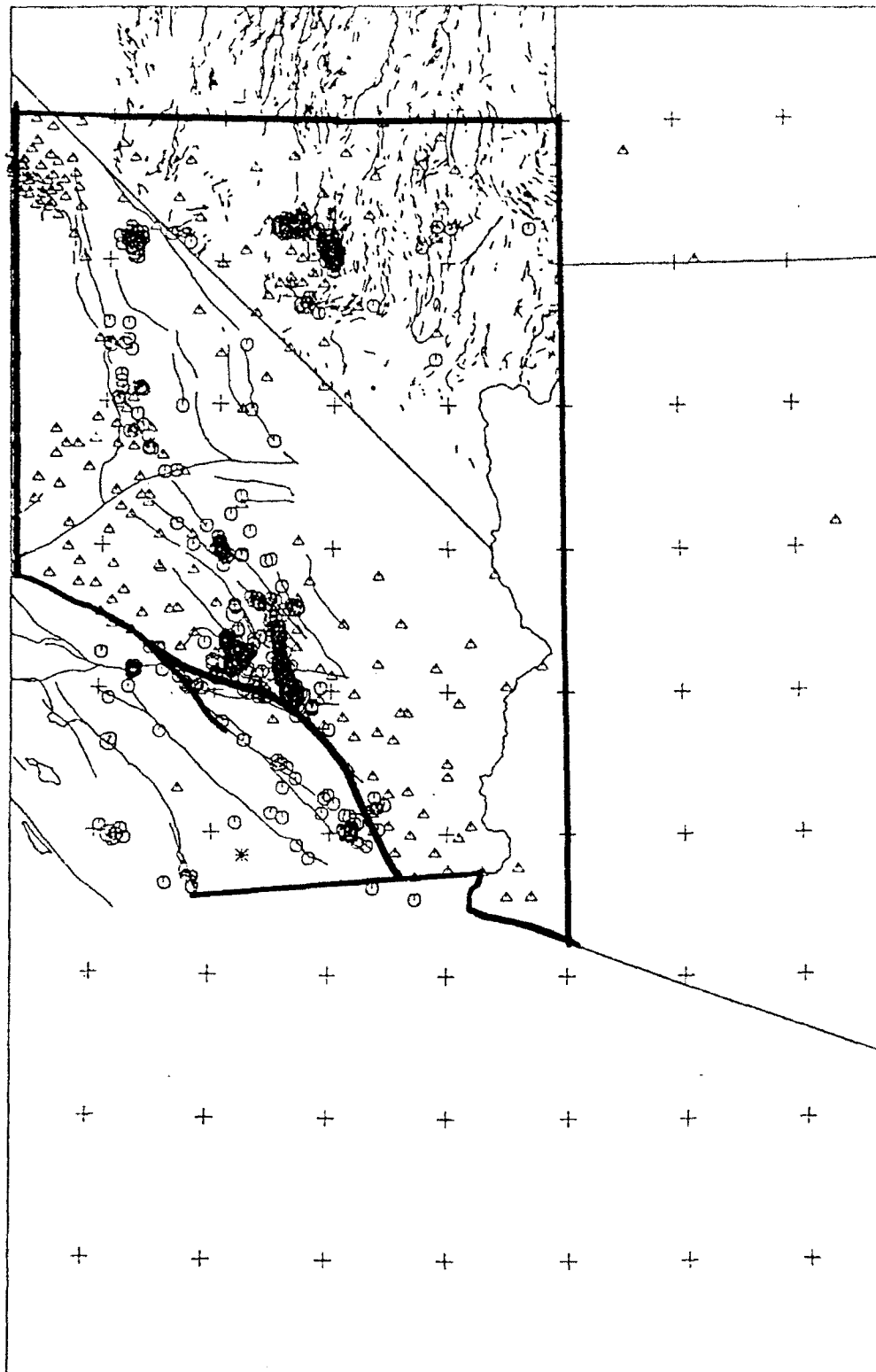


Figure 1: Study area for tomographic analysis is shown by bold line. P and S arrivals have been collected from seismic events (circles) that were recorded at the seismograph stations indicated by triangles.

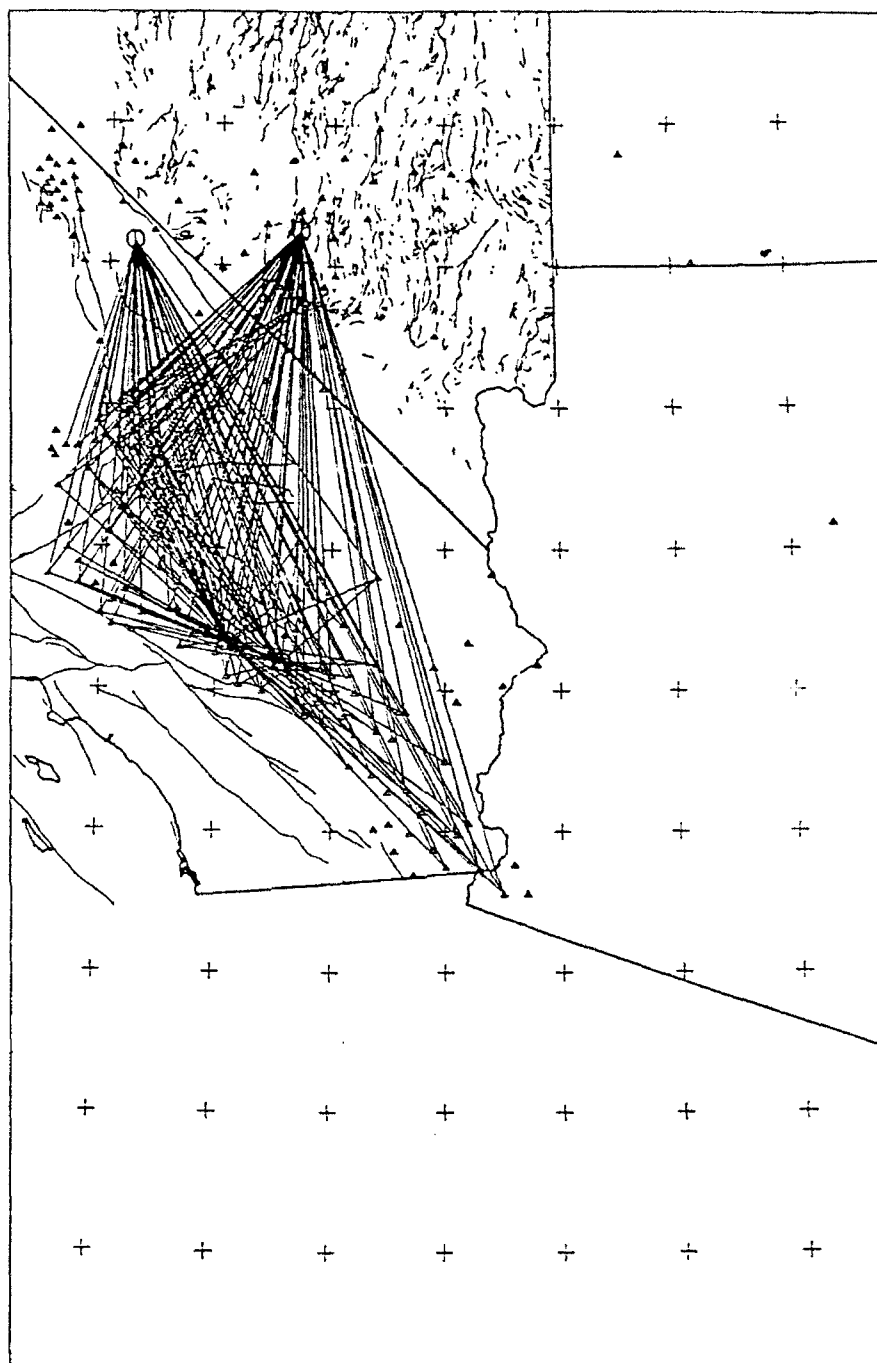


Figure 2: Example of seismic ray path coverage from several selected (magnitude < 5.0) seismic event within the study area.

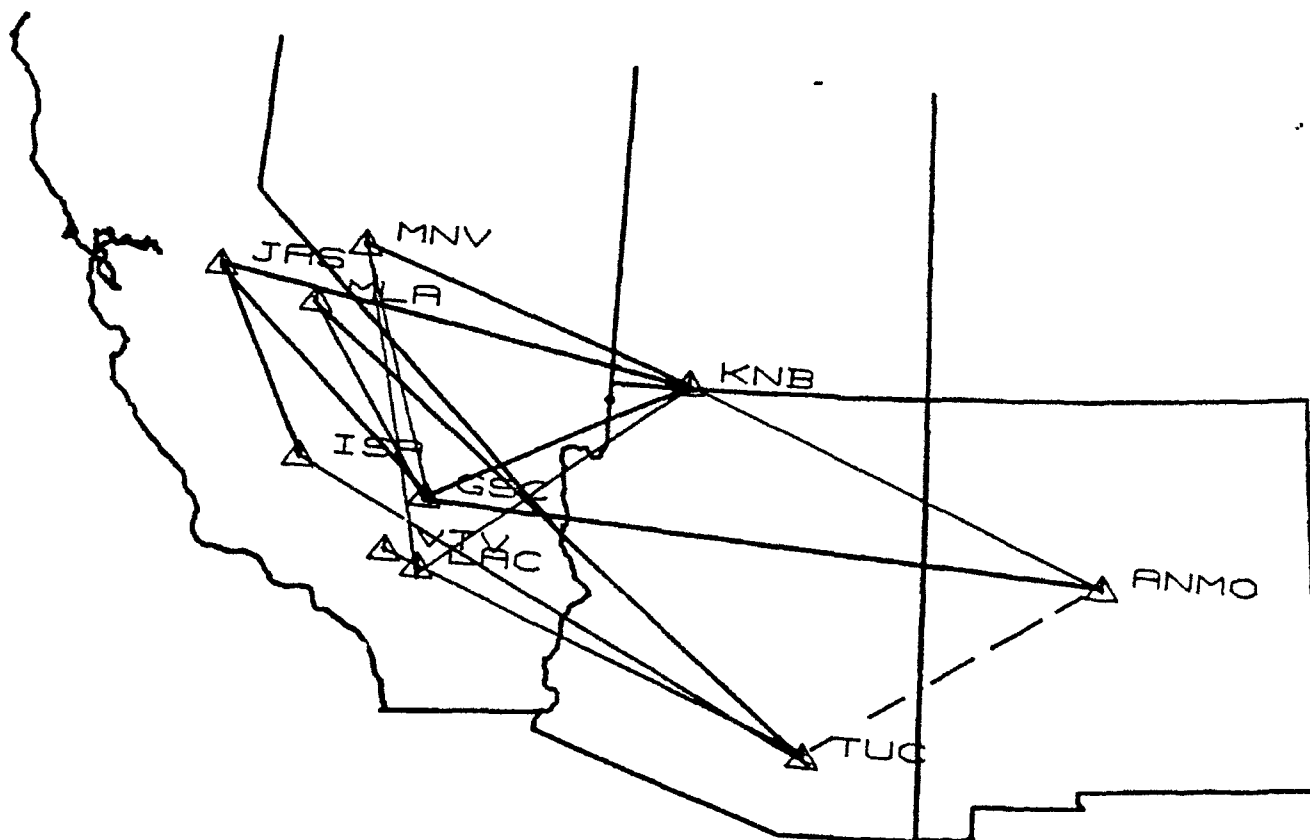


Figure 3: Seismograph stations (triangles) to be used in a surface wave study to determine regional variations in shear wave velocity. Great circle paths between stations of interest are shown by lines. The dashed line between ANMO and TUC is a path that has already been analyzed.

hand digitized. Two undergraduate students, Ms. Claudia Campos and Ms. Anabel Garcia, are working under the direction of Drs. Doser and Keller on this portion of the research.

Sierra Nevada Foothills Velocity Structure Determined from Local Earthquake Network Data

Funding from this grant has enabled Dr. Kate Miller to complete an earthquake study in the Foothills of the Sierra Nevada (Figure 4). Results of this work provide an important framework for the interpretation of data from the east-west transect of the upcoming Southern Sierra Nevada Continental Dynamics Project (SSCD) refraction experiment. Her study area lies immediately north of the SSCD transect. A summary of these Sierra Nevada Foothills results follow. A manuscript on these results is currently in revision for the Journal of Geophysical Research (Miller and Mooney, 1993). The Foothills Metamorphic Belt (Figure 4) is the long band of metamorphic rocks of Mesozoic and Paleozoic age that separates the Great Valley fore arc basin from the Sierra Nevada batholith in northern and central California. The belt is structurally complex, and has been alternatively interpreted as a Jurassic collisional zone or an intra-arc to forearc transtensional-transpressional shear system. Since the Foothills metamorphic rocks are also the country rock into which the Sierra Nevada batholith has intruded, late Mesozoic plutons are also important elements of the crustal structure at the southern end of the Foothills Metamorphic belt (Figure 4). The deep crustal structure and composition of the Foothills belt have not been extensively study, but are important to a complete understanding of the nature of the deep crust in central California. The presence of a microearthquake network and a seismic reflection profile at the southern end of the Foothills belt (Figure 4) permit the first real opportunity to simultaneously interpret the composition and structure of the crust within this terrane. Earthquake hypocenters occur at depths as great as 8 to 40 km (Figure 5) which makes the data set particularly useful for obtaining deep-crustal velocity information from seismic inversion techniques. In this study, a five-layer velocity model is determined from microearthquake travel-time data. The velocity model shows velocities of 5.2 to 6.3 km/s for the upper 12 km of the crust, and 6.7 to 6.8 km/s from 12 km to an estimated Moho at 32 km (Figure 6). The upper-crustal veloci-

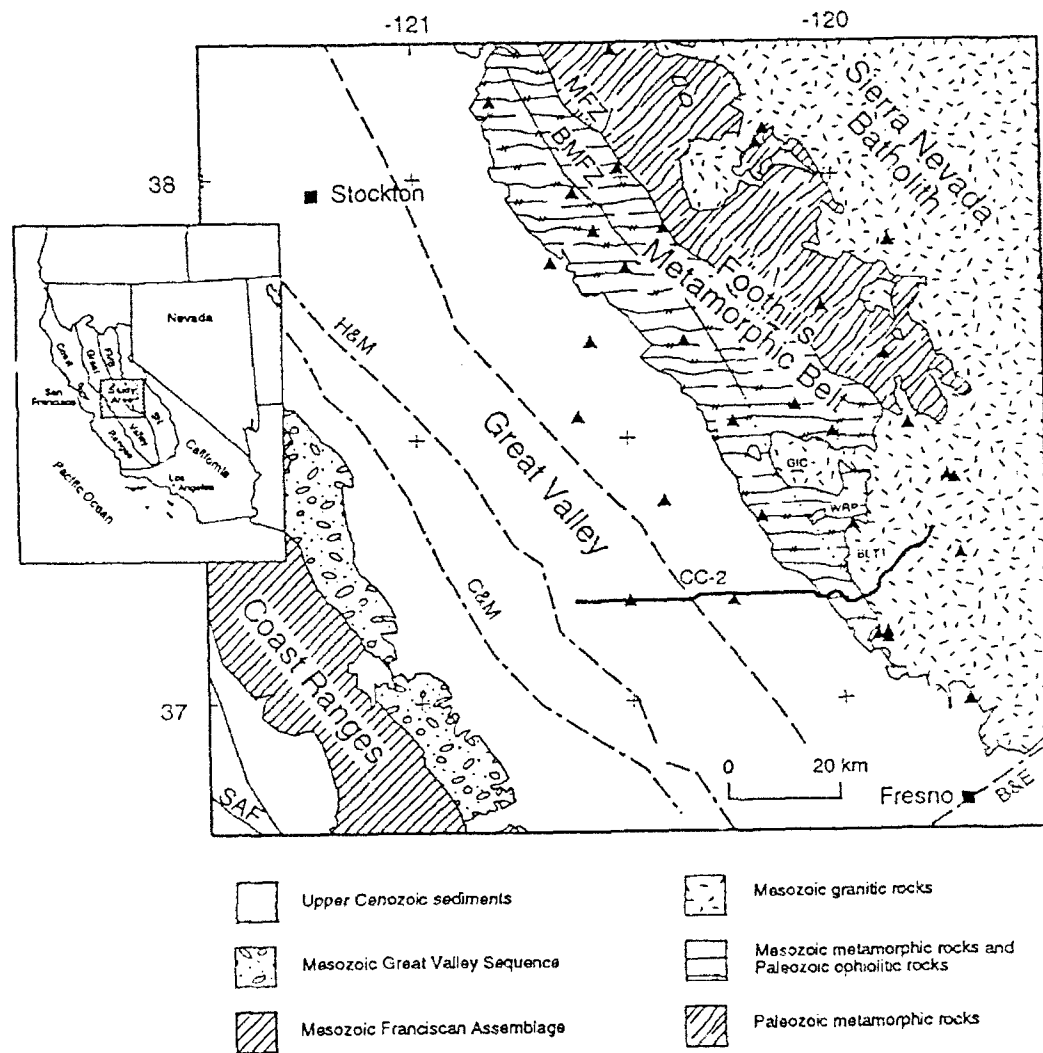


Fig. 1

Figure 4: Geologic map of study area. Chief rock units after Jennings [1977]. Abbreviations: MFZ – Melones Fault Zone; BMFZ – Bear Mountains Fault Zone; SAF – San Andreas Fault; GIC – Guadalupe Igneous Complex; WRP – White Rock Pluton; BLT – Bass Lake Tonalite. Solid triangles are earthquake station locations. Thick solid line is seismic reflection profile CC-2. Dashed line in the Great Valley is the axis of the steepest gradient on the northeast side of the Great Valley magnetic high. Dot-dash line are refraction profiles: B&E – Bateman and Eaton; C&M – Colburn and Mooney; H&M – Holbrook and Mooney

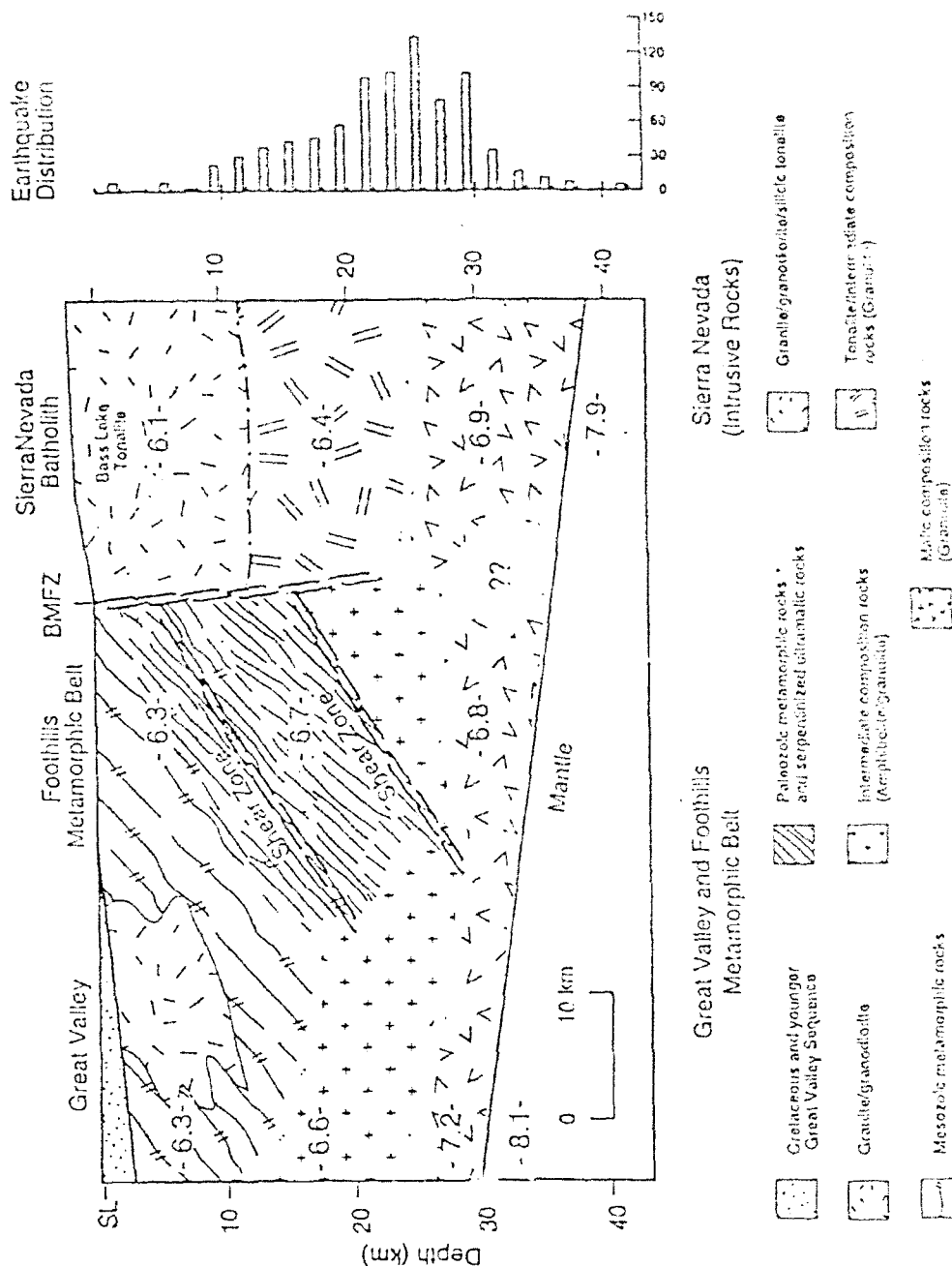


Figure 5: A schematic cross-section along the CC-2 transect. The sub-Foothills reflection pair are interpreted as shear zones formed during the late Jurassic Nevadan orogeny that were subsequently truncated by one of three mechanisms: 1) intrusion of batholithic rocks; 2) strike-slip faulting or; 3) reverse motion along the near-vertical shear zone that corresponds to the Bear Mountains fault zone. Note that earthquake epicenters occur at depths comparable to the shear zones.

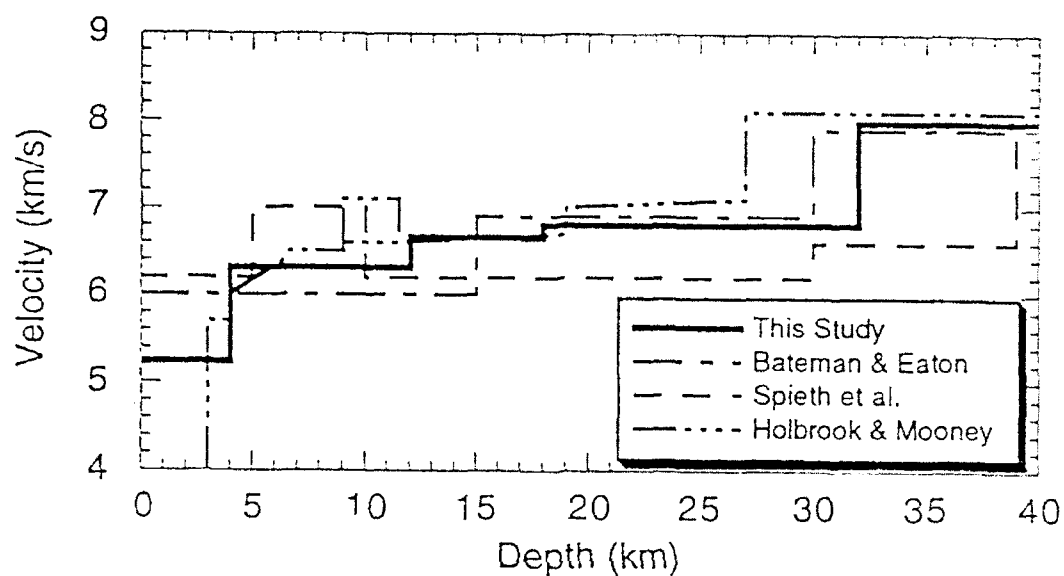


Fig. 2

Figure 6: Representative velocity–depth functions from refraction surveys and this study. Velocity models discussed in the text are: A) *Holbrook and Mooney* [1987]; *Colburn and Mooney* [1986]; B) *Spieth et al.* [1981]; C) This Study; D) *Bateman and Eaton* [1967]. Near 10 km depth in the *Holbrook and Mooney* model both the ophiolite and non-ophiolite velocities are shown.

ties correspond to Foothills metamorphic rocks and serpentinites as well as to diorites and granodiorites of the Sierran batholith, while the lower-crustal velocities are interpreted to represent intermediate to mafic granulites. The velocity results differ significantly from other Foothills results and from the Great Valley Province to the west (Figure 6). The low average velocities found in the upper 12 km of the 1-D velocity model are consistent with the complete disappearance of a high velocity layer seen in the Foothills and in the Great Valley. In its place, presumably, are variably serpentinitized peridotite with infolds of schists and metagraywackes of the Foothills Belt, and granites and granodiorites of the Sierran batholith. In the lower crust, velocities obtained in this study are comparable to those found beneath the Sierra Nevada batholith, but are significantly lower than those seen beneath the adjacent Great Valley. The majority of the earthquake hypocenters as well as a 6.7 km/s layer in the velocity model correspond in depth to thick zones of west-dipping mid-crustal reflections seen on seismic reflection profile CC-2, that may represent major shear zones formed during the late Jurassic Nevadan orogeny or syn-batholithic ductile shear zones that accommodated crustal extension associated with batholith intrusion. These reflections are truncated updip by an inferred sub-vertical contact that coincides with the western edge of the Sierra Nevada batholith and the southward trace of the Bear Mountains fault zone. Figure 5 is a schematic cross-section showing this interpretation with earthquake distribution.

Upper Crustal Structure of Northern Arizona Using Inversion of Pg Travel-Times From the 1989 Pacific To Arizona Crustal Experiment (PACE)

Experiment Description

In order to obtain a better understanding of the tectonic history and crustal structure of the CP, a seismic study completely confined within the CP was felt necessary. Therefore during the PACE experiment (Figure 7), data was collected along an approximately 230 km long crossline profile located within the CP. This crossline profile extended in the NW-SE orientation from the north rim of the Grand Canyon to northeast of Flagstaff, Arizona (Figure 7). This profile included 7 small in-line and 3 large off-end shots. These shots were recorded by different portable instrument types; including vertical component seismic cassette recorders (SCR's), vertical component seismic group recorders (SGR's), and vertical component PRS-1's.

Out of 470 instruments, 350 were placed at 100 m spacing centered about the tie point of the mainline (Plateau) and crossline (Grand Canyon) profiles. The 7 small in-line shots were evenly spaced, about 5 km apart, across this distance. The rest of the 470 instruments, total of 120, were deployed at 500 m spacing to extend the profile northwest and southeast. This geometry allowed recording of detailed wide-angle reflection data from the entire crust and possibly the upper mantle. Because of the closely spaced shots and dense receiver array, the experiment provided high resolution data.

PACE-1989 Data Description

The refraction data recorded during PACE-1989 along all the profiles are of high resolution throughout the study area. This was achieved by close spacing of both shots and receivers. Since the development of any seismic model depends on the identification of various phases, a brief description of the data and various travel time phases is given here.

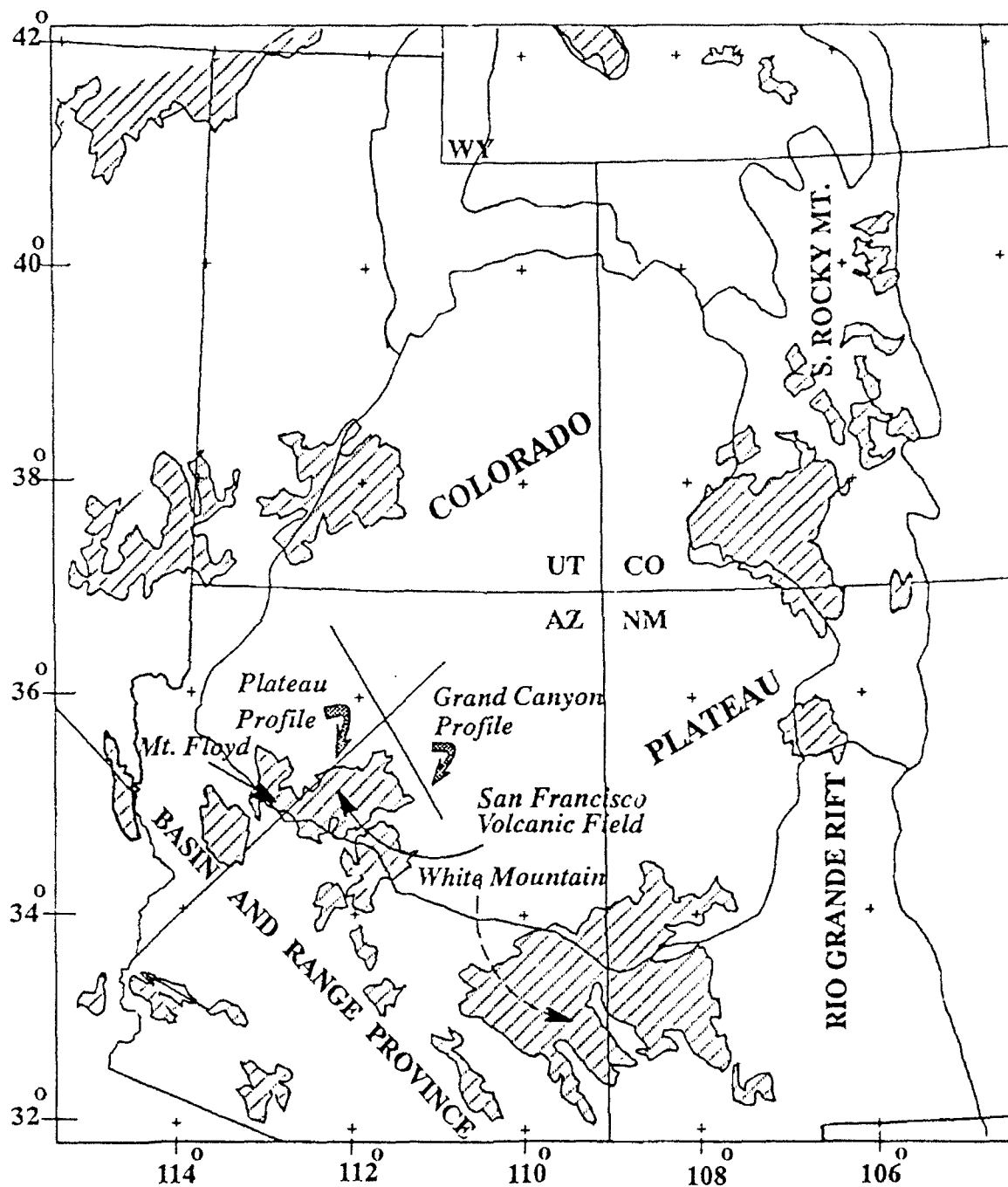


Figure 7: Map showing the location of PACE-1989 mainline (Plateau) and crossline (Grand Canyon) profiles. Volcanic centers are shaded.

Refractions through the highly fractured, low velocity, sedimentary rocks are observed up to offsets of 6.0 km on all the shots recorded. The apparent velocities of these arrivals are highly variable and range between 2.0 km/sec to more than 5.0 km/sec. Thickness of this layer was modeled only close to the shot points and interpolated to farther distances.

The upper crustal Pg arrivals which bottom in the Precambrian basement typically have velocities of 6.0 km/sec and 6.2 km/sec. The Pg refraction phase is very strong between offsets of > 6.0 km and 100.0 km after which these are either not observed or obscured by high frequency noise. The Pg velocity increases to more than 6.3 km/sec in areas of mafic intrusions into the upper crust.

A total of 1504 Pg travel time picks were made from the seismic sections up to offsets of more than 100 km. No Pg arrivals were picked from the southeastern most shot point 82 because the nearest receiver was more than 74 km away from the shot point and the Pg phase could not be clearly recognized. The Pg travel time picks were easily recognizable on the rest of the seismic sections and were of high quality. The Pg arrivals were assigned an estimated average picking error of 0.05 seconds.

Travel-Time Inversion

Until recently, the interpretation of seismic refraction/wide angle reflection data involved only a tedious and painstaking trial and error ray-trace forward modeling approach. This approach requires that the model's theoretical response be compared repeatedly with the observed data until a velocity model is obtained that provides a suitable match between the observed and the calculated response. At best, this requires countless person hours because of many iterations required to reach a suitable model. On the other hand, seismic inversion techniques are relatively fast and can provide estimates of model uncertainty, resolution, and non-uniqueness, but inversion techniques are not always robust and the parameterization of velocity structure is restricted to simple geometries.

The inversion technique used for this study was developed by Zelt and Smith (1992, *Geophys. J. Intl.*) and was used by them for similar crustal studies. This inversion technique is iterative and is based on a model parameterization and a method of ray tracing suited to seismic refraction/wide angle reflection data. The velocities and interfaces are defined as specified nodal points to suit the shot-receiver geometry, subsurface ray coverage, and details of the near surface structure. The stability of inversion is improved by applying a smooth layer boundary simulation to a blocky model parameterization. Rays are traced through the velocity model using zero order asymptotic ray theory by solving the ray tracing equations numerically. The partial derivatives of travel time with respect to velocity and the depth of boundary nodes are calculated analytically during ray tracing. Rays are traced through each group of arrivals and travel times and partial derivatives are interpreted across the two closest ray end points. The parameter values selected for adjustment, both velocities and boundary nodes, are simultaneously updated using a damped least-squares inversion. The inversion process is stopped when either the final model is achieved with the desired trade-off between Root-Mean-Square (RMS) travel-time residual and parameter residual, or rays are traced to all observations. The inversion method is particularly suited to multishot crustal seismic refraction/wide angle reflection data which would otherwise be forward modelled.

Seismic record sections of 4 of the 10 shot points along the Grand Canyon profile are shown in Figures 8, 9, 10, and 11. These data are for shot points 83, 85, 76, and 77, respectively.

The inversion of the PACE-1989 data was carried out in four successive steps. First, the upper crustal Pg data was inverted for velocity and upper crustal thickness. Second, the mid-crustal reflection data, PiP phase, was inverted while keeping the upper crustal velocities and thickness fixed. The same procedure was adapted in inverting PmP phase, reflections off of the Moho and PtP phase from within the mantle. This procedure was adapted to speed up the inversion algorithm and obtain error estimates of the velocities and depths of individual layers. Since the velocities and

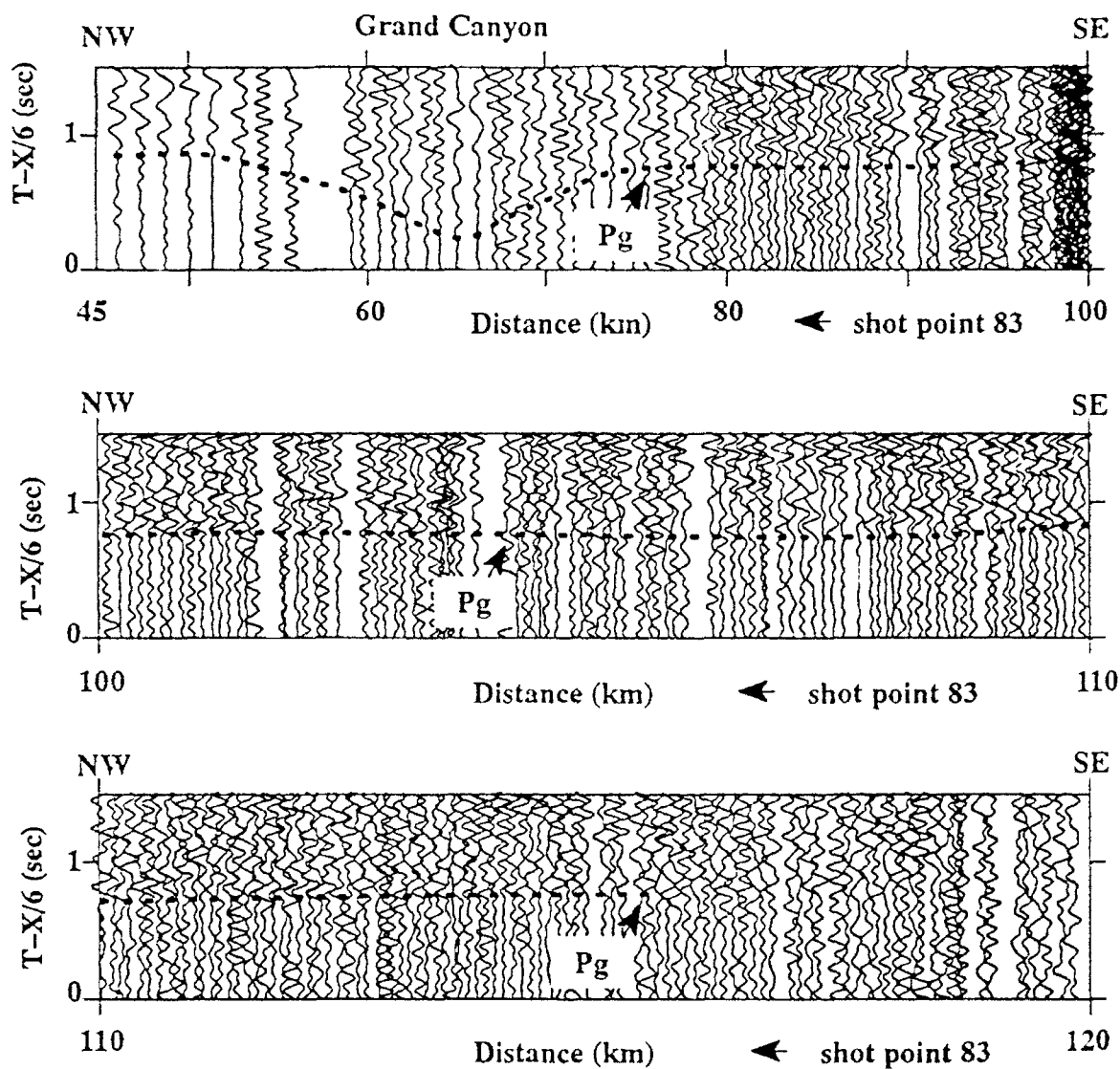


Figure 8: Seismic record showing the upper crustal Pg arrivals for the crossline shot point 83.

The vertical axis is reduced travel-time with reduction velocity of 6.0 km/sec while the horizontal axis is shot-to-receiver offset in kilometers. The traces have been plotted with a maximum trace amplitude normalization. The panels are plotted with variable offsets due to variable receiver spacing in the field. The upper crustal Pg arrivals for shot points 85, 76, and 77 are shown in Figures 9, 10, and 11, respectively.

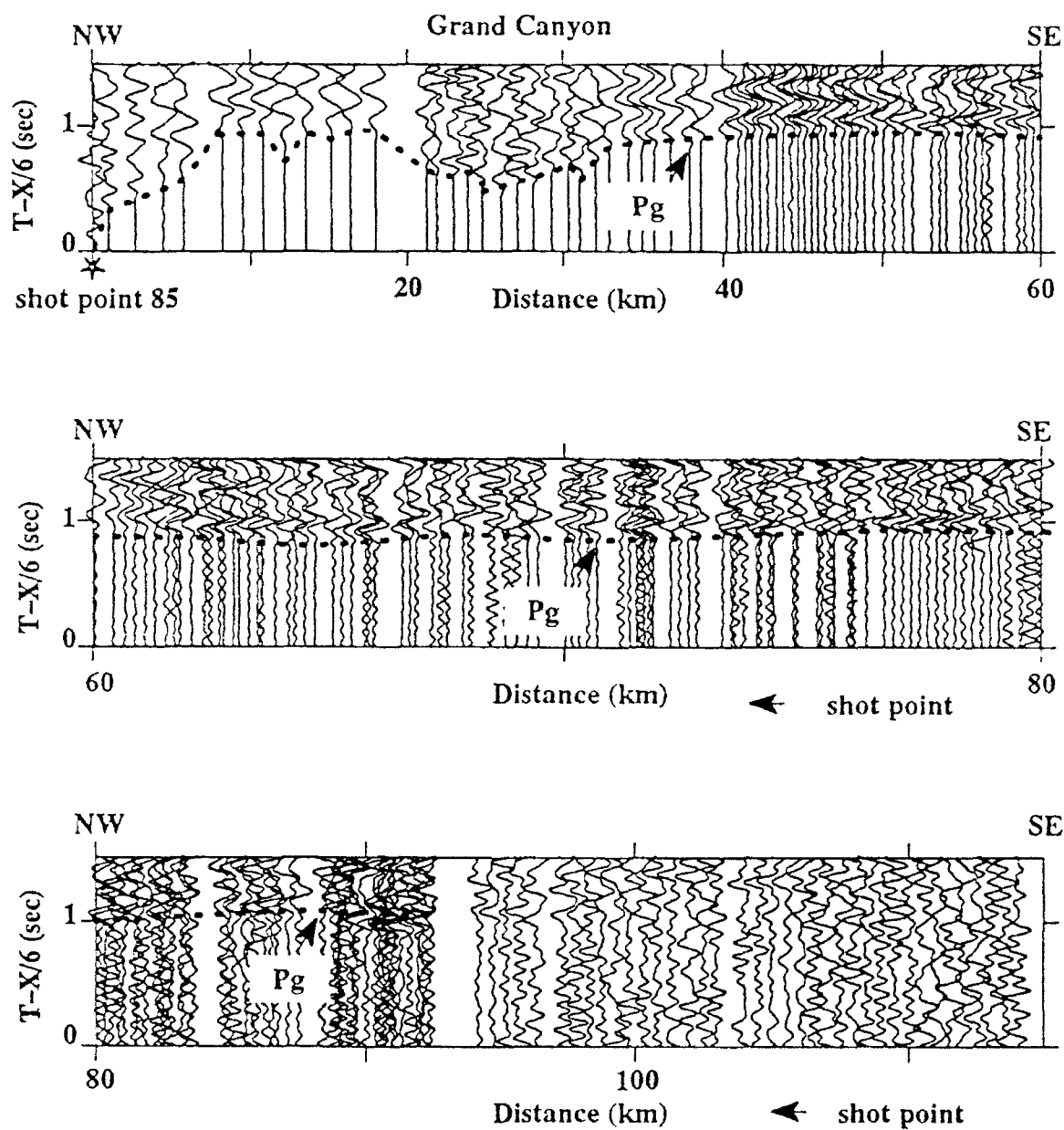


Figure 9: Seismic section for shot point 85. See Figure 8 for details.

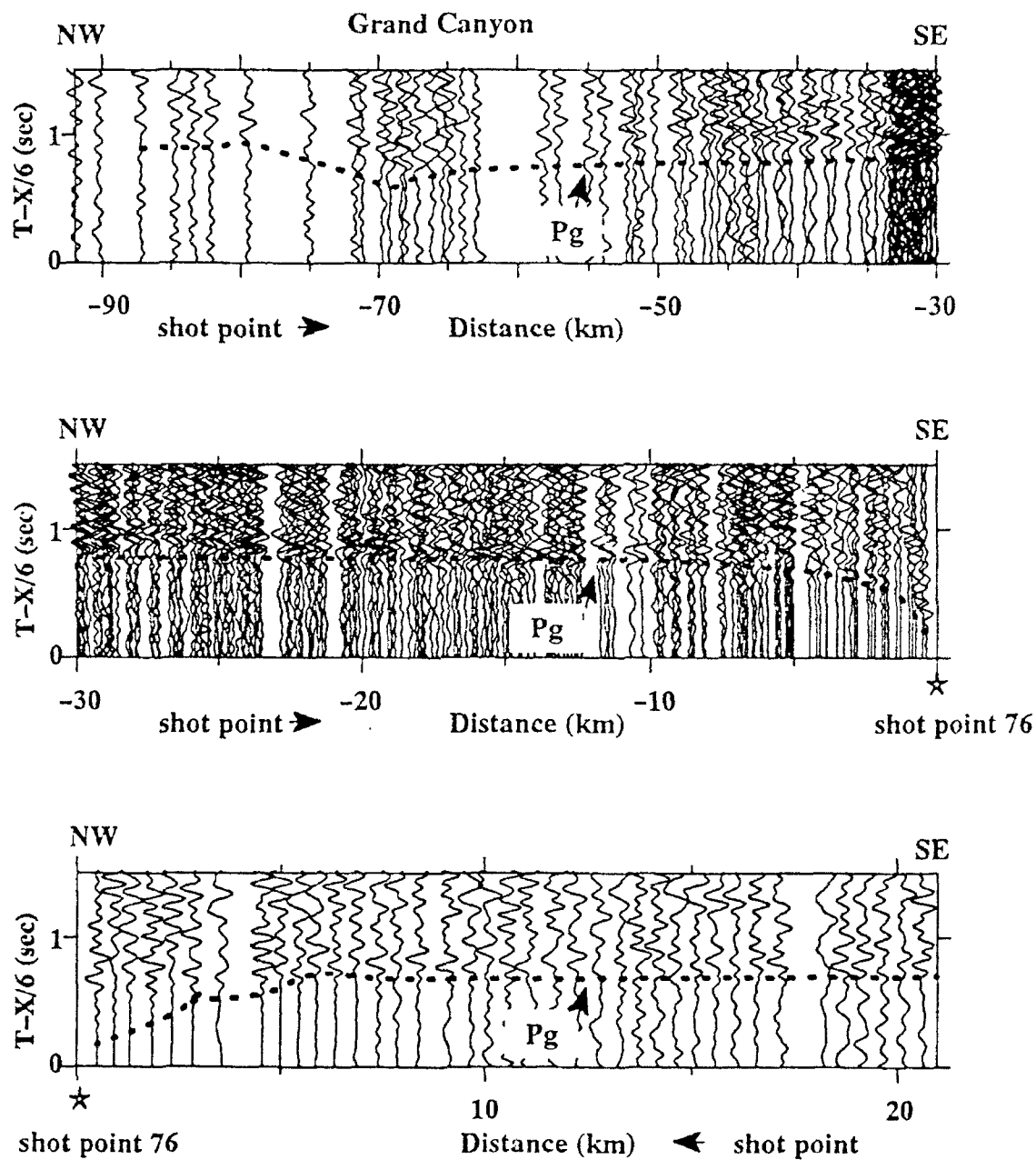


Figure 10: Seismic record for shot point 76. See Figure 8 for details.

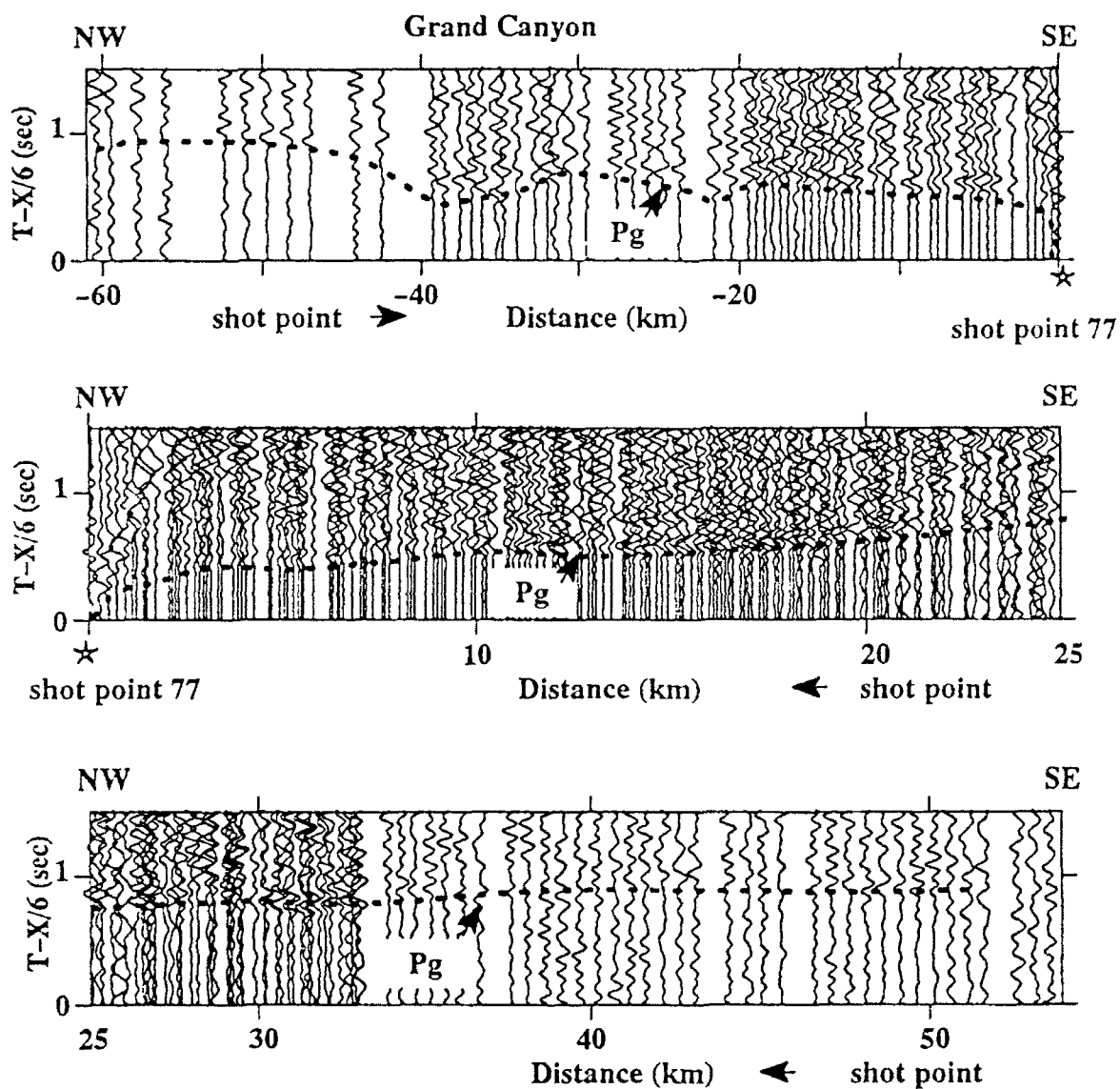


Figure 11: Seismic record for shot point 77. See Figure 8 for details.

depths of a bottom layer has no effect on the velocity and depth of the layer above it, this procedure was found most useful. A flat-layer, constant velocity starting model was used in each of the steps described above. The earth structure obtained in step 1 was held fixed in step 2 and the structure in steps 1 and 2 was held constant in step 3 and so on. Since the surface topography in the study area was added in the model as the top most interface, no corrections were made to the data for surface topography or near-surface velocity variations. The elevations and depths in the seismic model are with respect to the mean sea level with positive values below sea level.

The cumulative inversion result of the upper crustal Pg arrivals for the entire crossline is shown in Figure 12. For reasons of clarity, the model derived from the inversion is plotted for individual shots. Examples included are for shot points 83, 85, and 76, respectively (Figures 13, 14, and 15).

In general, the thickness and velocities of the final model are well resolved with a Root Mean Square (RMS) error close to the error assigned to the travel time picks (0.069). The travel time fit is good ($N^2 = 0.211$) and rays were traced to almost all arrivals.

Discussion

The inversion result for the upper crust can be subdivided into two separate layers with velocities varying from 2.0 km/sec to more than 5.0 km/sec in the thin, less than 2.0 km thick sedimentary layer and about 6.0 km/s in the Precambrian basement.

The upper low velocity, sedimentary layer is of variable thickness with thicknesses varying from less than 0.5 km towards southeast to about 1.5 km towards northwest. This layer is observed on all shots and contributes significantly to the travel time delays observed in the data.

The Precambrian basement (upper crust) could be modeled in detail to depth of about 10 km and contained significant velocity variations. The velocity at the upper boundary of this layer varies

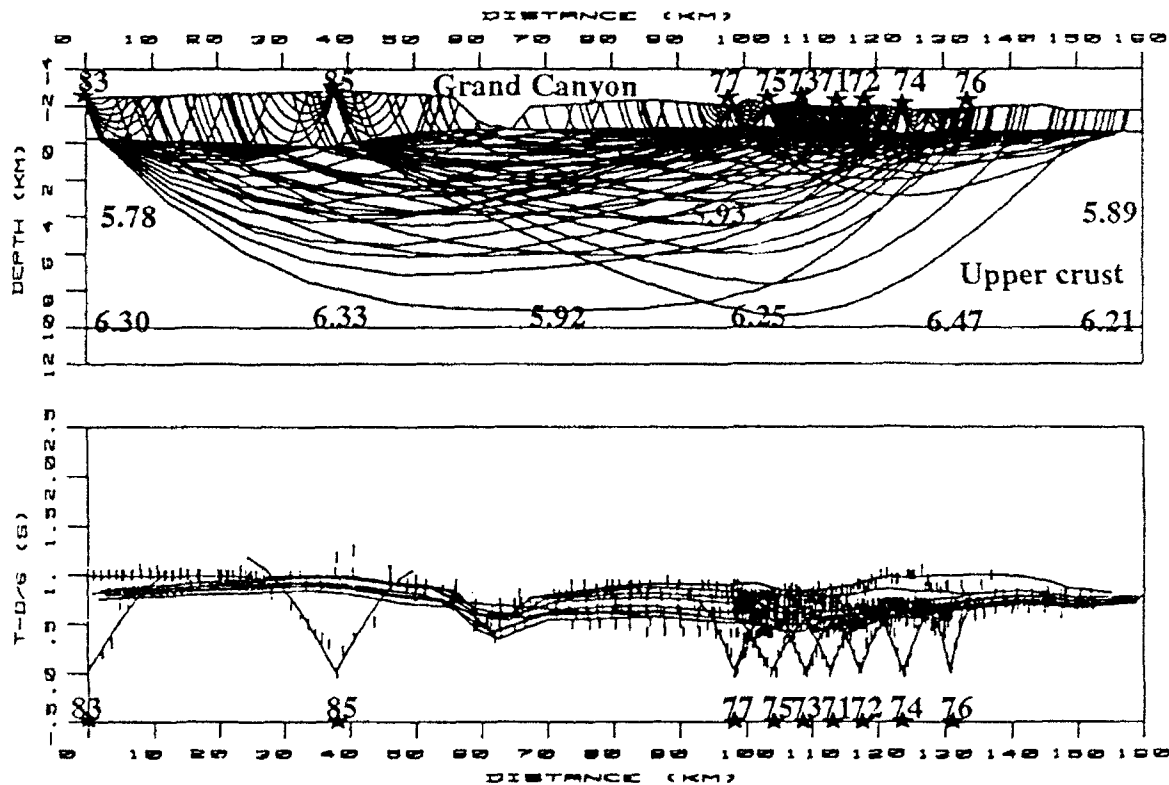


Figure 12: Cumulative result of the upper crustal velocity model across the PACE-1989 Grand Canyon profile derived from Pg arrivals using Zelt inversion algorithm.

Upper panel shows the velocity structure of the upper 10 km of the crust while the lower panel shows the match between observed (vertical bars) and calculated (solid line). The data in lower panel is plotted with reduction velocity of 6.0 km/sec.

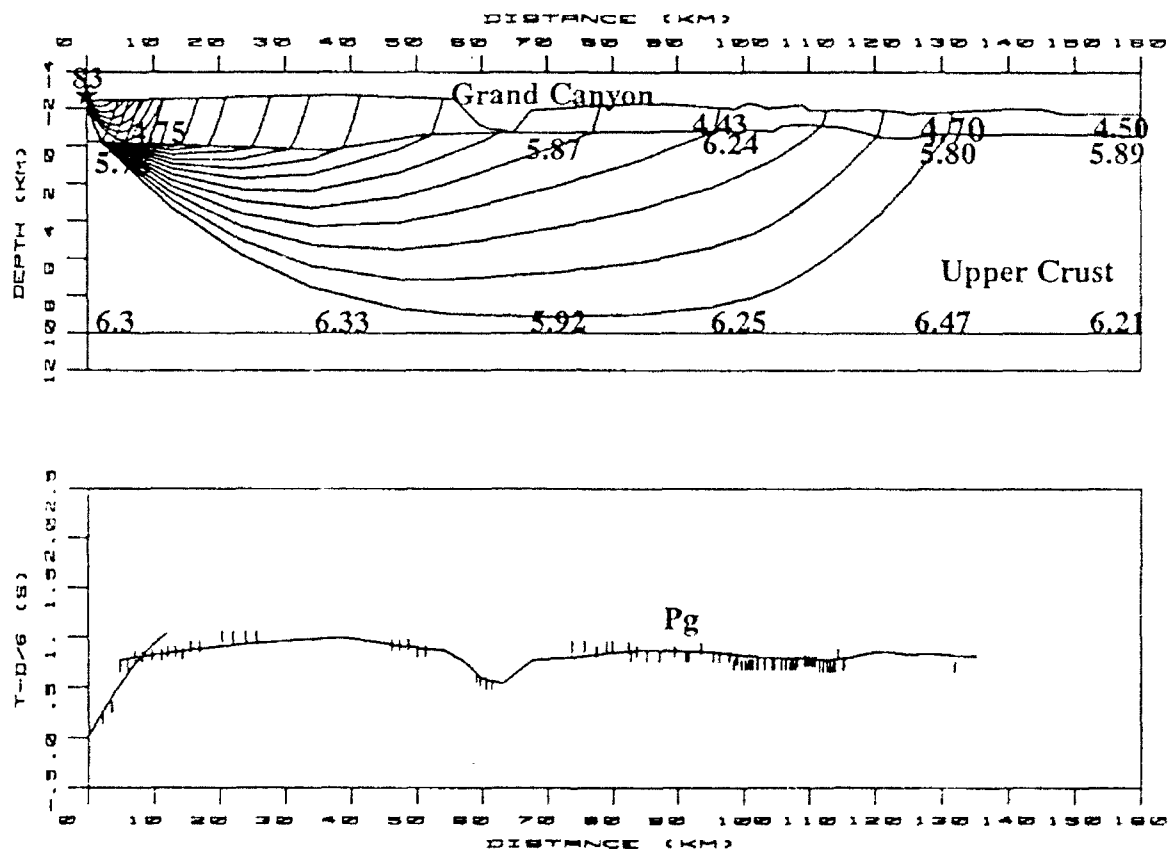


Figure 13: Upper crustal velocity model for shot point 83 across the PACE-1989 Grand Canyon profile derived from Pg arrivals using Zelt inversion algorithm.

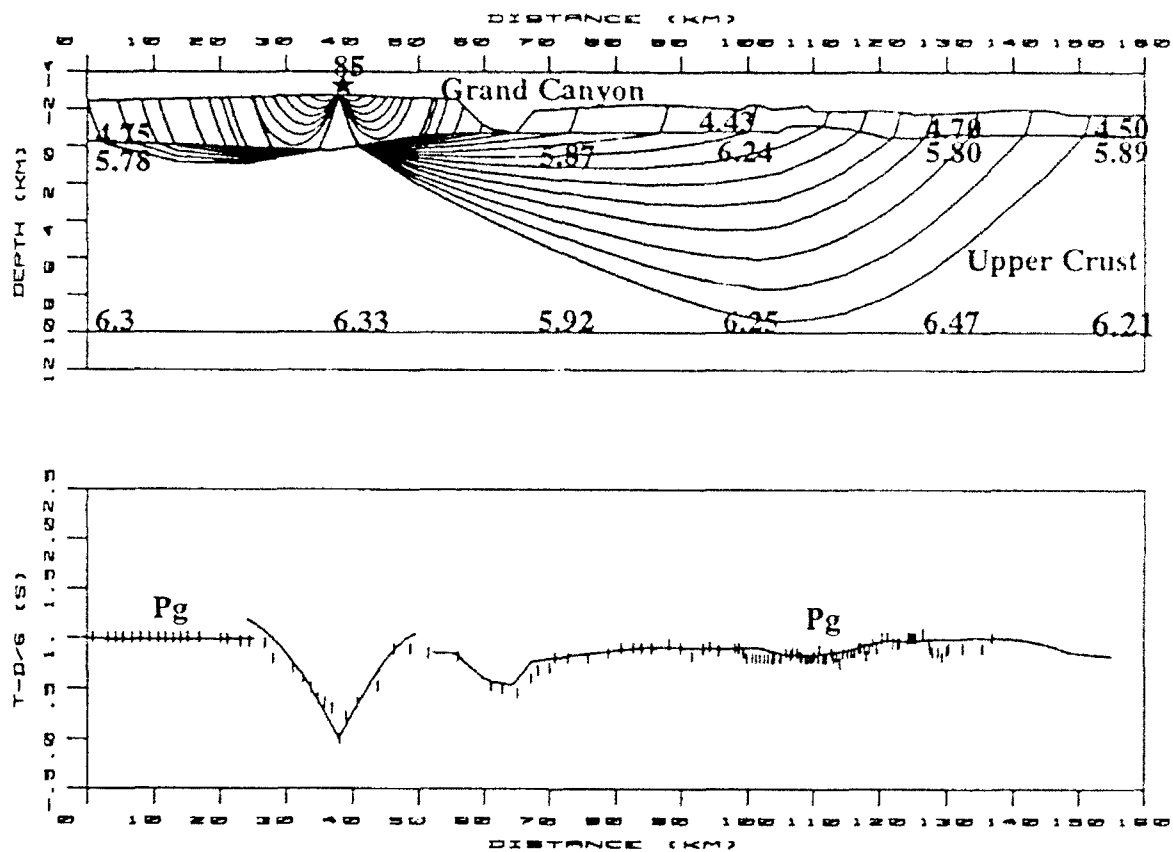


Figure 14: Upper crustal velocity model for shot point 85 across the PACE-1989 Grand Canyon profile derived from Pg arrivals using Zelt inversion algorithm.

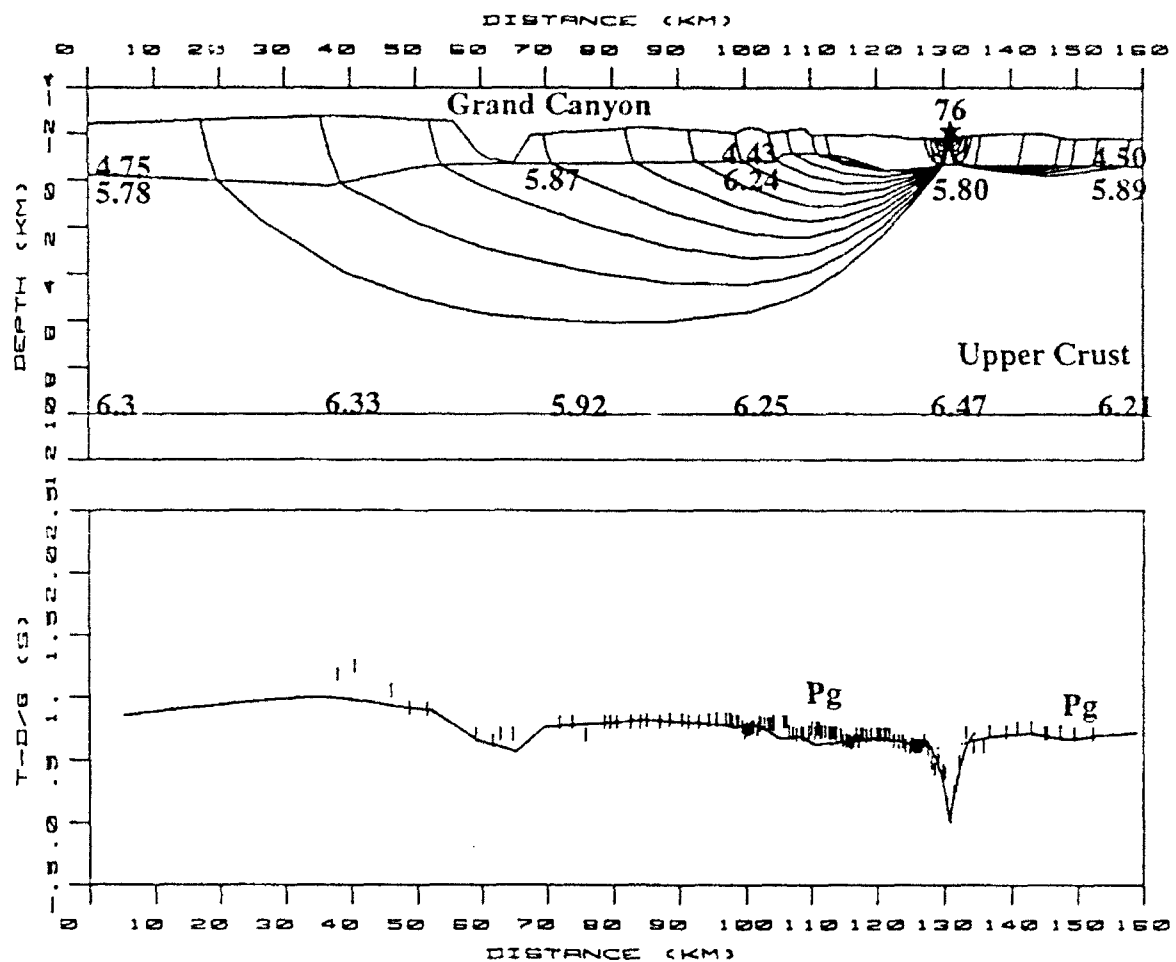


Figure 15: Upper crustal velocity model for shot point 76 across the PACE-1989 Grand Canyon profile derived from Pg arrivals using Zelt inversion algorithm.

from 5.5 km/sec to about 6.0 km/sec while the velocity at the lower boundary varies from 6.1 km/sec to about 6.4 km/sec. The rays bottoming in this layer, the Pg arrivals, are observed from offset of 5-10 km to offsets of greater than 100 km.

The inversion results are in good agreement with the geologic data in the area. The velocity variations observed in the Precambrian basement can be interpreted in a geological context. The low velocity zones are interpreted as areas where the Late Proterozoic Chuar Group makes up the upper portion of the basement. This clastic unit outcrops in the Grand Canyon and has been encountered in several wells in the area. The high velocity zone under shot point 76 could be due to the presence of the Late Cenozoic San Francisco volcanic field. This area is also seen as a gravity high on Bouguer anomaly maps. The velocity values obtained also correlate well with the velocities obtained by analysis of sonic logs in wells in the SFVF and surrounding areas.

Three-Dimensional Velocity Structure of the Upper Crust Under the San Francisco Volcanic Field, Arizona, From Pg Arrival Tomography

Description of the PACE-1989 Parallel Seismic Profile

The 1989 Pacific to Arizona Crustal Experiment (PACE) included two seismic refraction/wide angle reflection profiles crossing each other near Flagstaff, Arizona). Two shorter profiles (Figure 7) were also recorded to provide some control on basement velocities. Profile 3 was deployed by the University of Texas at El Paso group and consisted of an array of 22 single component seismic instruments in a line parallel to the PACE-1989 mainline. These instruments recorded all the shots along the PACE mainline, and the seismic energy crisscrossed through the SFVF. Two off-end shots were also recorded on the receivers along the mainline and produced seismic waves that also traveled through the SFVF. The ray coverage through the SFVF (Figure 16) provides an excellent opportunity to employ three-dimensional tomographic techniques to study the seismic properties of the field. The purpose of this study is to investigate the possibility of an upper crustal magma chamber beneath San Francisco Mountain and O'Leary Peak and the evidence for a region of increased partial melt in the upper crust beneath the volcanic field that would serve as a source for the numerous basaltic vents.

The Seismic Tomography Technique

Tomography is defined as the method of reconstruction of an object from its projections. This problem was first considered in detail by Radon in 1917 in a landmark paper. Inverse techniques based on the Radon transform are particularly useful for equally spaced data sets, such as controlled seismic refraction experiments, since fast Fourier transform techniques can be implemented. Radon's theorems can be directly applied to uniquely invert for the image of the object through which the specific rays are traveling. In seismology, the travel times can be represented as the line integral of the slowness (inverse of velocity) profiles along the specific ray paths. Tomogra-

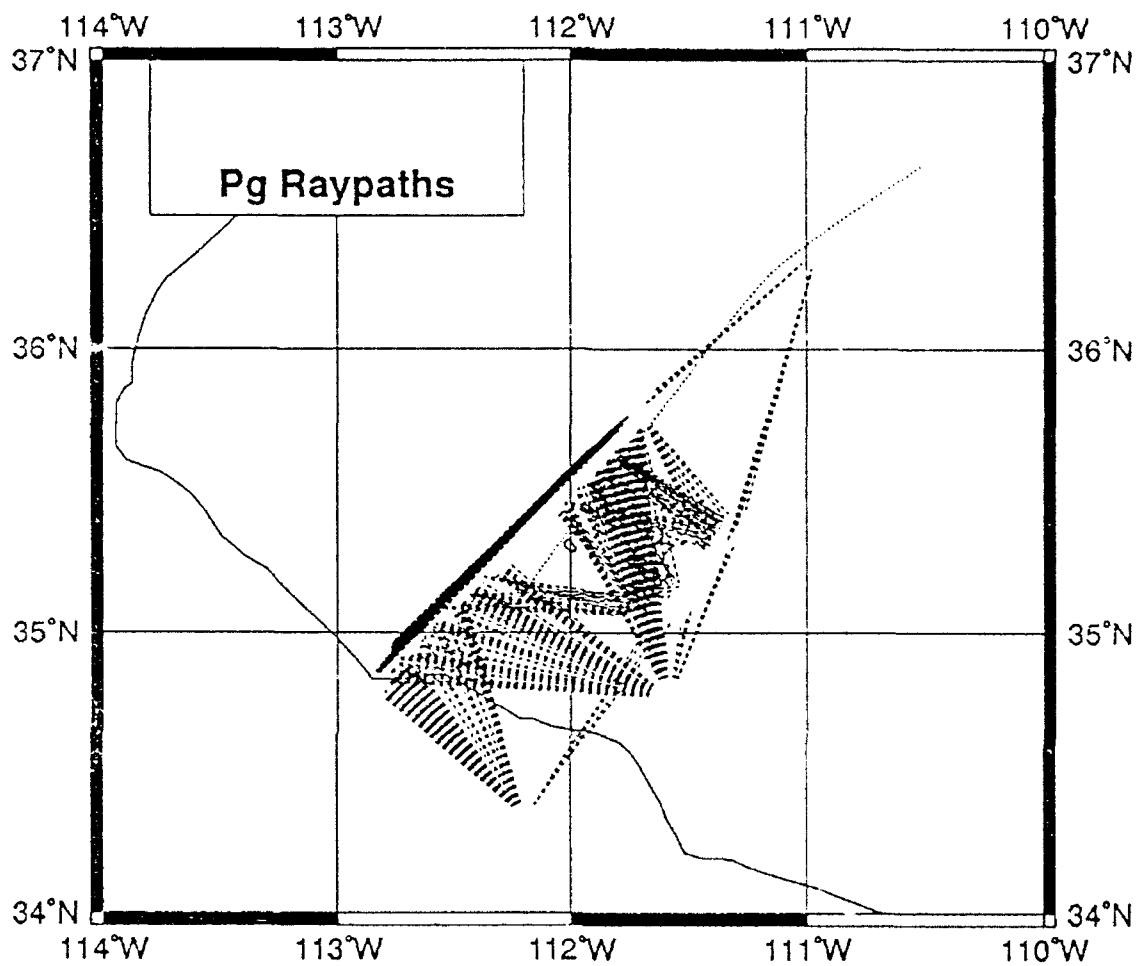


Figure 16: Ray coverage diagram showing ray paths through the San Francisco volcanic field.

phy has found applications in a wide variety of scientific fields such as medical (X-ray, ultrasonic velocity, or gamma ray intensity), astrophysics (radio astronomy data), planetary science (occultation data), and geophysics (velocity inversion). The inversion of travel times into structure is the problem of imaging an object from its projections. In this study, the time term method of seismic refraction is used to tomographically determine the slowness image and refractor topography of the upper crust under the San Francisco volcanic field.

The time term method of seismic refraction was first introduced in the 1950's. Thomas Hearn has recently developed an expanded form of the time term method which could be used to determine delay times, lateral velocity variations and regional anisotropy, and we have worked closely with him to implement his technique in this study. The time term method separates the residual travel time of a refracted ray into three parts corresponding to the source delay, the station delay, and the horizontal distance between source i and station j . The equation giving the travel time of a seismic wave through a structure consisting of two materials separated by a plane interface (Figure 17) may be written in the form:

$$t_{ij} = a_i + b_j + \frac{\Delta_{ij}}{v} \quad (1)$$

where a_i and b_j are "time terms", (also referred to as delay times or time intercepts) for the sources and receivers, respectively, Δ_{ij} is the distance between the shot-point and the seismograph, t_{ij} is the time of propagation of a refracted wave, and v is the velocity of uniform underlying "marker bed". Equation (1) is linearized by using the slowness instead of its reciprocal velocity, and can be written as:

$$t_{ij} = a_i + b_j + \Delta_{ij} S \quad (2)$$

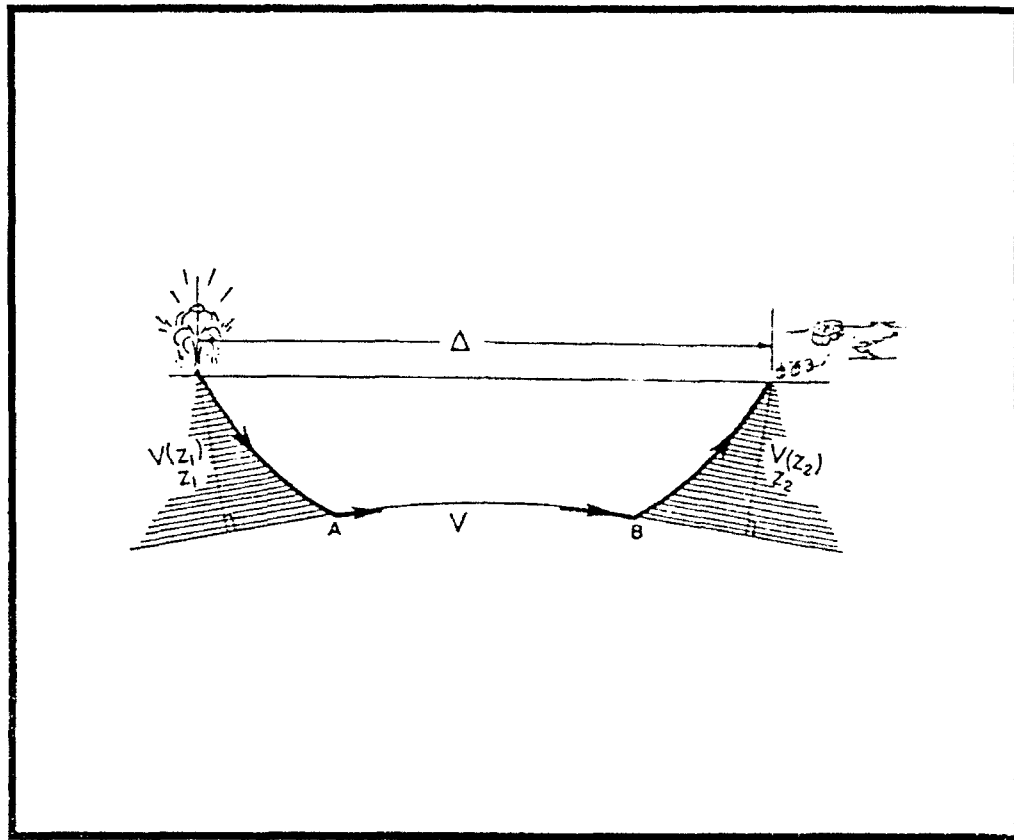


Figure 17: Propagation of a seismic wave in a two-layer medium.

where S is the refractor slowness. The station and source delays could be expressed in terms of refractor depth h , refractor slowness S , and the slowness depth profile, $S(z)$.

$$a_i = \int_0^h (S(z)^2 - S^2)^{\frac{1}{2}} dz \quad (3)$$

$$b_j = \int_z^h (S(z)^2 - S^2)^{\frac{1}{2}} dz \quad (4)$$

If m recording stations observe waves from n sources, up to $n \times m$ equations of type (1) may be obtained. The problem is then to determine the best value of the velocity v and the time terms for all sources and stations. Finally, the time terms can be interpreted in terms of the corresponding depths h , so that the contours of the interface can be obtained. The advantages of the method are that the equations can be solved without requiring the shot points and stations to be laid out in any particular pattern, the maximum amount of information is extracted from the data, and the requirements for making simplifying assumptions about the geological structure (assumptions which are, for example, involved in describing the structure in terms of plane layers).

The area under investigation is divided into a grid of cells of equal length and width. Each ray is traced across the grid and weighted sums of delays and slownesses are kept for each cell, station, and event involved with that ray. After all of the rays are used, the mean delays and slownesses are calculated. This process is called back projection, since each travel time is projected back along its ray path. Because data are traced sequentially, there is no limit on the amount of data that can be used. The computed delays depend on both the crustal velocity profile and the refractor slowness, while the station delays depend on both the depth of the refractor and the velocity profile above it. An independent knowledge of crustal velocities is desirable to separate these two effects. However, the delay estimates can be corrected for variations in refractor velocity by assuming a

constant offset distance, the horizontal distance that the ray travels from the refractor to the station.

This offset distance can be calculated by expanding equation 3 by Taylor's series which gives:

$$a_i(s_0) = a_i(s_0 + \delta s) - \frac{\partial a}{\partial s_0} \delta s_0 \quad a_i(s_0)$$

$$a_i(s_0) = a_i(a_0 + \delta s) + \frac{s_0 h}{\sqrt{s_0^2 - s^2}} \delta s$$

$$a_i(s_0) = a_i(s_0 + \delta s) + F \delta s$$

where

$$F = \frac{s_0 h}{\sqrt{s_0^2 - s^2}} = 13.0 \text{ km}$$

The parameter F is dependent upon the unknown velocity profile, therefore, it is approximated by a constant value of 13 km. This value assumes an average upper crustal velocity of 5.5 km/sec, a refractor velocity of 6.0 km/sec, and a refractor depth of 5 km. The velocity and depth estimates of the upper crustal layer and the refractor depth used here as input were obtained from two-dimensional inversion of the data along the crossline. All station statics are corrected to this constant offset value. The corrected delays obtained are interpreted as either refractor depth or crustal velocity variations (slownesses). In the case of a constant velocity crust of $v_0 = 5.5$ km/sec, and refractor velocity of $v_1 = 6.0$ km/sec, an $a_0 = 0.1$ sec of relative delay corresponds to:

$$h = \frac{v_0 v_1 a_0}{\sqrt{v_1^2 - v_0^2}} = 1.4 \text{ km}$$

of refractor topography. In the case of a flat reflector, the same delay will correspond to a 0.5 km/sec upper crustal velocity change.

The estimated slownesses will be interpreted to delineate areas of positive and negative delays associated with an increase or decrease in the crustal velocities.

Tomographic Imaging of the SFVF Using Pg Arrivals

Due to the short shot-receiver offset along the parallel line, the majority of the arrivals passing through the SFVF were identified as upper crustal Pg arrivals. In this study, data processing was started by picking Pg arrivals from the travel-time data. This amounted to more than 4,000 arrivals. Pg phase picks between 13 km and 160 km were windowed and plotted on a time-distance plot and a straight line was fitted to the data. The outliers of more than 1 sec from the straight line fit were removed. The data in Figure 18 are plotted with the reduction velocity of 6.0 km/sec, which is the inverse slope of the line fitted to the data. The tomographic process is iterative. In the first step, the delays, slowness image, and the scaling factors (one to multiply all the event delays, one to multiply all the station delays, and one to multiply the slowness image) were calculated. After this, new residuals were calculated. These residuals were then back projected, and the resulting slowness perturbations were added to the previous estimates. This process was repeated until the change in the Root Mean Square (RMS) error was very small. All results shown here are for fifteen iterations. The slowness results are shown in Figure 19, and the associated delays are shown in Figure 20. The mean intercept and the inverse slope of the line fitted to the data in Figure 18 is 0.64 sec and 6.0 km/sec, respectively. The mean velocity perturbations in Figure 19 are ± 0.25 km/sec. This velocity range agrees well with the velocities obtained by two-dimensional inverse modelling of the data set along the crossline profile. The mean station delays are very small (0.003 sec). Negative delays, denoting

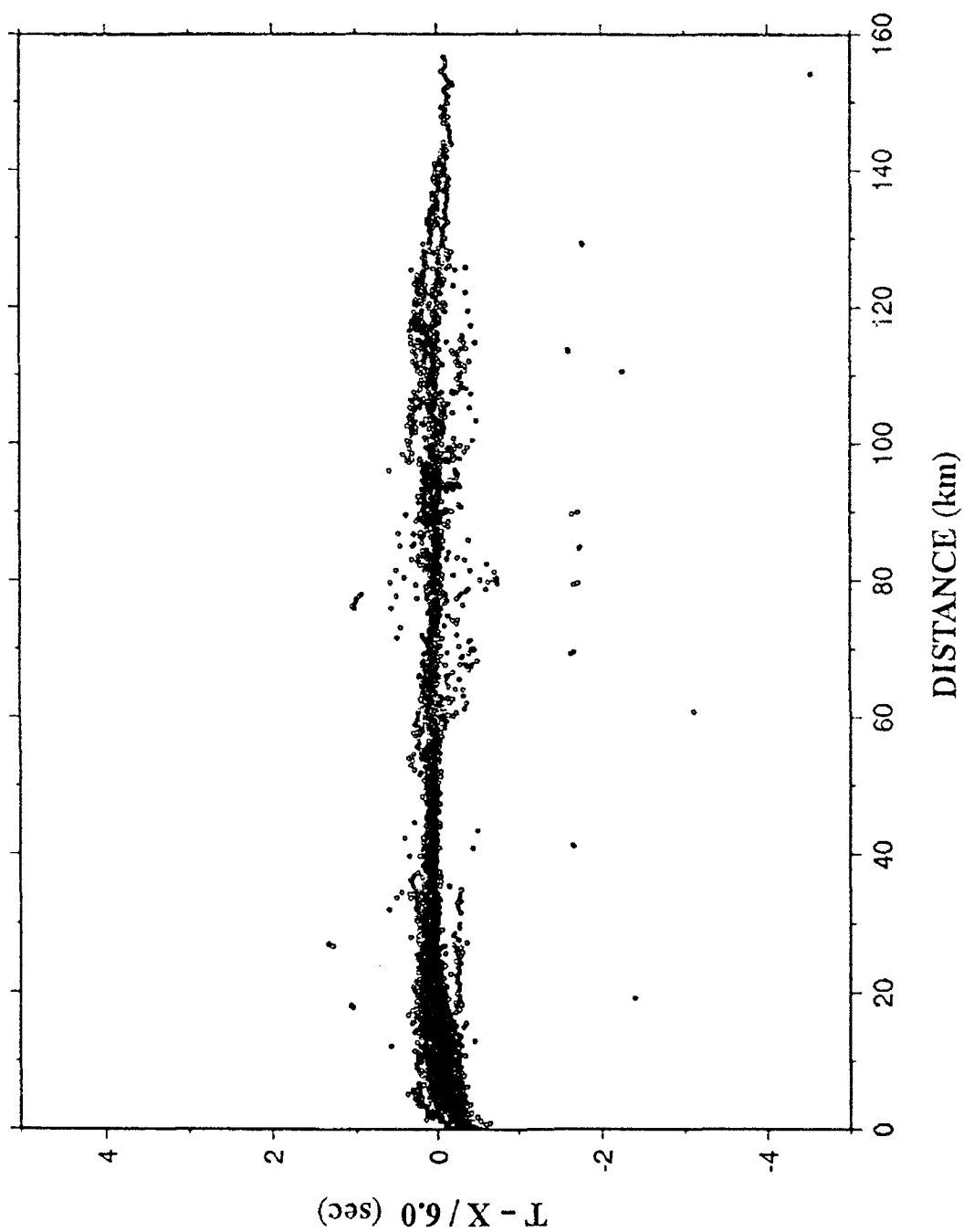


Figure 18: Pg travel-time pick are plotted as a function of source to receiver offset.

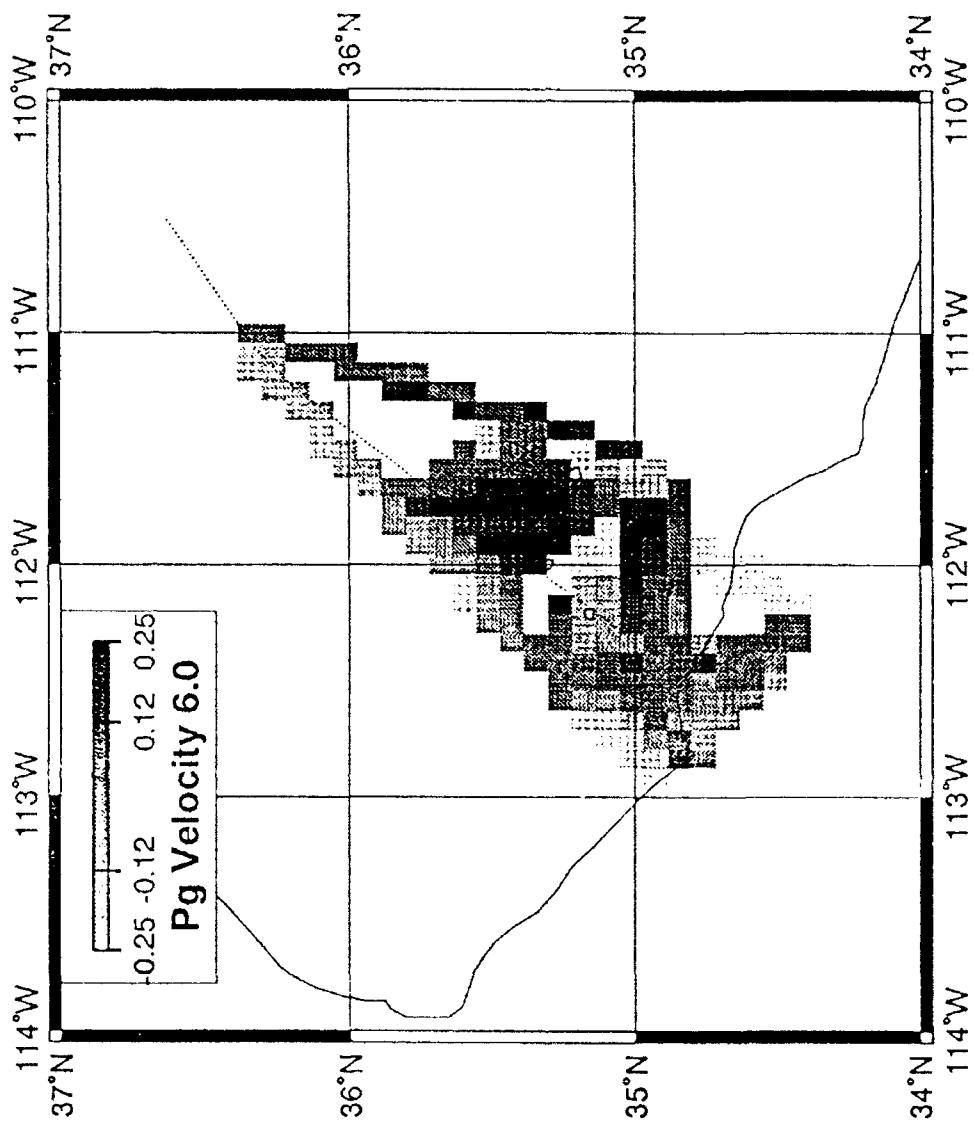


Figure 19: Slowness image result.

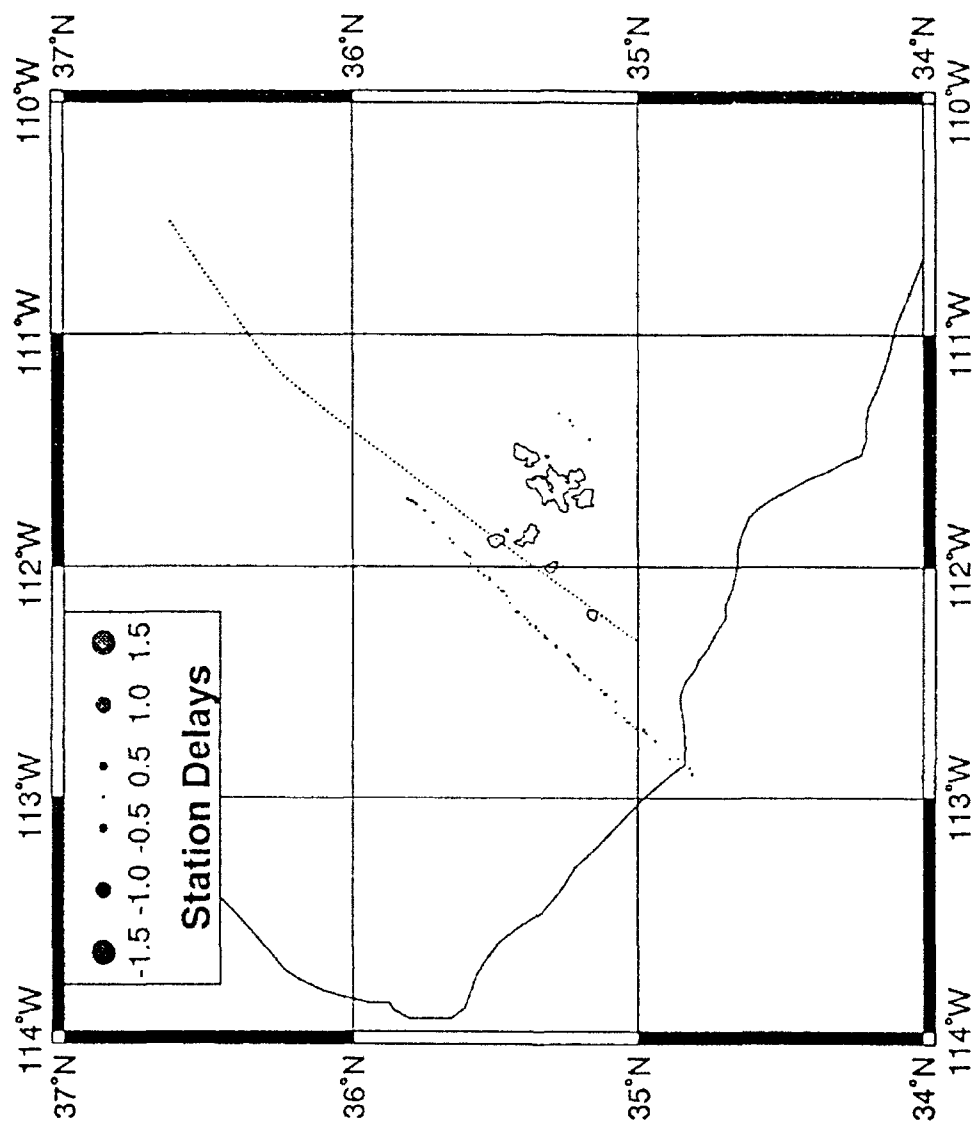


Figure 20: Inversion result of the noise static station delays.

early arrivals, are observed towards the edge of the parallel line closer to the southeastern boundary of the SFVF.

The quality of the solution obtained is determined by inverting artificial travel times and then inverting a synthetic model. This allows us to empirically investigate the resolution and variances of the slowness image obtained for the actual data. By applying the tomographic algorithm to these artificial travel times, the variance of the velocity values determined can be estimated. Instead of actual arrival times, travel times that have a Gaussian distribution with a standard deviation of 0.055 sec assigned to the highest quality arrivals, were used. This is a large amount of error. The actual ray paths of the data set were used in the reconstruction. The result of inverting these synthetic data indicate that Figure 19 is a reliable depiction of the upper crustal velocity variations in the area.

Discussion

The most significant feature of the tomography result in Figure 19 is the zone of high compressional velocity at upper crustal depths (less than 10 km) below San Francisco Mountain. The higher upper crustal P_g velocities of 6.3 to 6.9 km/sec correlate well with intermediate to basaltic rocks of the San Francisco volcanic field. The higher upper crustal velocities suggest the intrusion of magmas of basaltic composition into the upper crust below San Francisco Mountain stratovolcano as the volcano formed. If most of the dikes and sills that have intruded the upper crust in the SFVF have cooled below their solidus temperatures, the average velocity of the intruded region would be higher than the highly fractured and more silicic basement rocks surrounding it. The high upper crustal velocity of 6.7 km/sec to 6.9 km/sec under the San Francisco Mountain compare well with experimentally derived P -wave velocities for gabbros at upper crustal pressures. Gabbro, the intrusive equivalent of basalt, has P -wave velocities of 6.83 km/sec near the surface to about 6.99 km/sec at depths of 30 km. The high velocity regions also correlate well with positive gravity anomalies.

Summary

The time term analysis technique provides reasonable velocity structure of the San Francisco Volcanic field. High velocity zones are detected under San Francisco Mountain, and O'Leary Peak extending within 4 km of surface to about 7 km in depth. The P-wave velocities within these zones are from 5% to 14% higher than the surrounding basement rocks. These high velocities could be caused by the intrusion of numerous mafic dikes and sills into upper crust, cooling to subsolidus temperatures while the volcanic centers grew. Gravity modeling of the San Francisco Volcanic field indicates that the high velocity regions are coincident with the high density bodies at upper crustal depths under many of the volcanic centers. It could, therefore, be said with confidence that the high velocities found here are evident in various data sets that have been interpreted independently of each other.

Long Offset Profile Across the Rio Grande Rift and its Transition Zones in Central New Mexico

A number of geophysical surveys have been conducted over the last 20 years to examine the intra-rift structure and morphology of the Rio Grande Rift (RGR). The purpose of this research is to expand on these previous studies by using long offset seismic data to examine the transition zone between the southern RGR and the neighboring Great Plains (GP) province to the east. The profile of recordings begins southeast of Socorro, New Mexico and extends eastward to near the Texas-New Mexico border (Figure 21). The surface expression of rifting within this region is postulated to extend as far east as the western extreme of the Sacramento and Pedernal Uplifts but no seismic investigations have examined the transition at depth.

The profile was chosen so it would have a near radial orientation to the Nevada Test Site (NTS). The large nuclear explosions created at NTS provide excellent seismic sources and the resultant long offsets (> 1000 km) make it possible to examine the structure of the transition region to depths below the low velocity zone in the upper mantle. The investigation targeted these depths because it is presumed that the RGR-GP transition extends into the deep lithosphere and asthenosphere.

However, these long offsets also present a problem. Since the ultimate objective of the survey was to analyze the rift/craton transition zone, a modeling technique that allowed for two-dimensional velocity structures was necessary. The method chosen for this survey was a 2-D ray tracing algorithm based on asymptotic ray theory (ART). In addition, since all of the station offsets in this work were over 900 km, some type of compensation had to be made for the curvature of the earth. Conventional earth "flattening" transforms involve various mathematical techniques for modifying a homogeneous, flat earth model so that the results obtained from the specific modeling algorithm approximate those expected from a homogeneous, spherical earth. The two-dimensional nature of

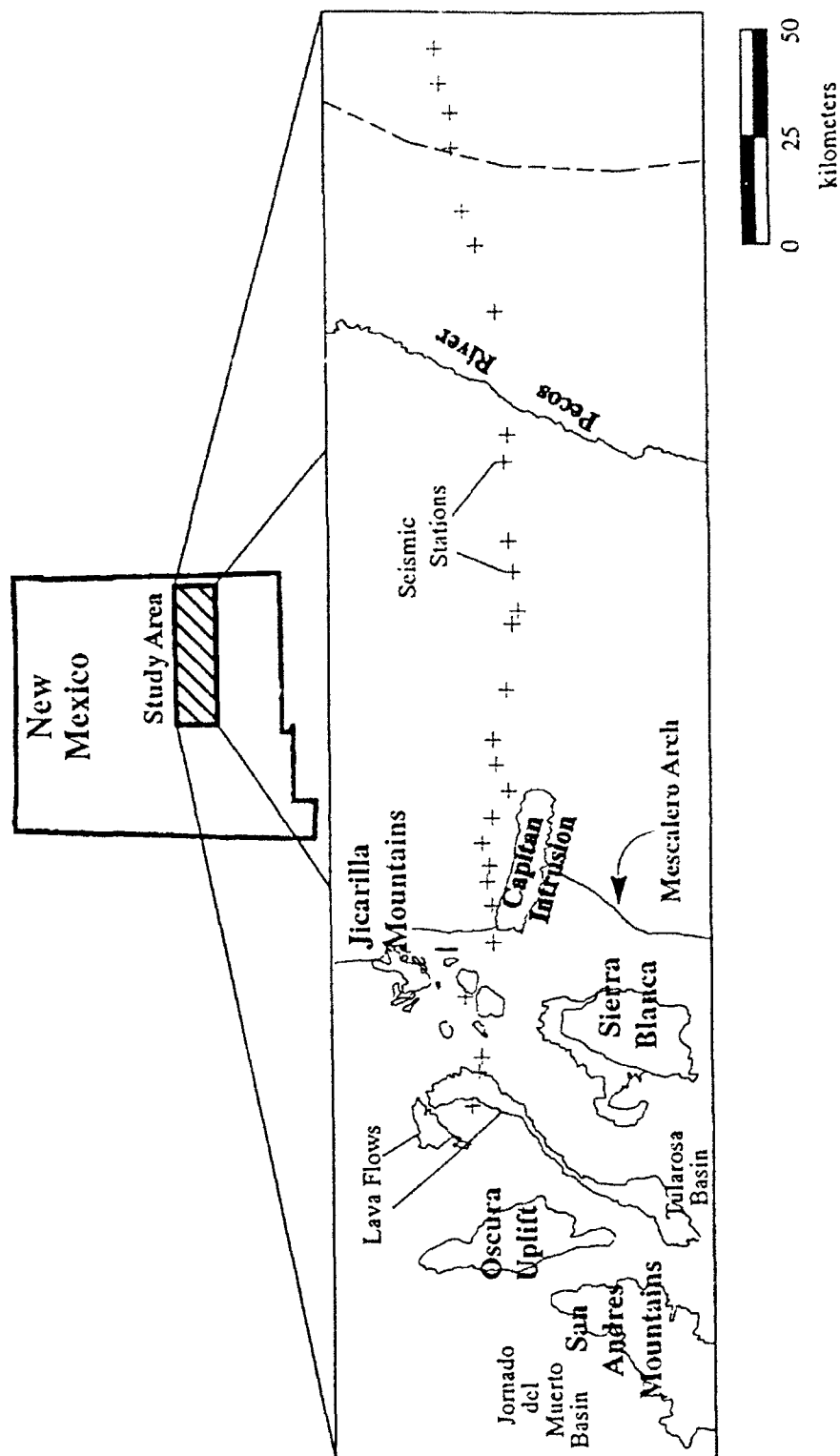


Figure 21: Geologic setting of the study area.

The dashed line at the eastern end of the figure corresponds to the refraction line of Stewart and Paiser (1962).

the models used in ART make the application of such a transformation difficult. To alleviate this problem, a new technique of compensating for the curvature was developed for this study.

We implemented a geometric solution to the curvature problem: the earth was approximated by a series of pie-shaped wedges. Within each of these wedges, the earth was assumed to be flat, but the cumulative error in this assumption is small if the pie wedges are kept small, e.g. about 50 km. A true Cartesian coordinate system is set up with the X -axis tangent to the earth's surface at the center of the user's model and with Y increasing towards the center of the earth. Each of the interfaces in the user's "flat-earth" model space is divided into a series of line segments, and then each of the endpoints of the line segments is transformed from the user's coordinate system into the true Cartesian system using the mathematical relationship described in Figure 22. The result is a series of curved surfaces drawn in a truly Cartesian coordinate system.

The modeling algorithm then proceeds, using the (X, Y) coordinate system, to determine the appropriate ray paths and travel times. Each ray is stopped at the boundary corresponding to the earth's surface (as opposed to $Y=0$) and the final (X, Y) coordinates are inverse transformed to determine the range at which the ray exited the model. The accuracy of this technique was tested by comparing the its output with that predicted by conventional earth flattening algorithms using a homogeneous, layered earth model. Careful observation of these data show that this approach accurately predicts the arrival times to distances of greater than 1000 km.

Analysis of Seismic Sections

The seismic sections gathered during this work are displayed in Figure 23. The first arrivals across both sections are interpreted as P_n : critical refractions from the Moho discontinuity. The second arrival is P_1 : an arrival refracted below the upper mantle low velocity zone. Synthetic sections generated using a standard earth model for the region suggest that several phases with arrival times of

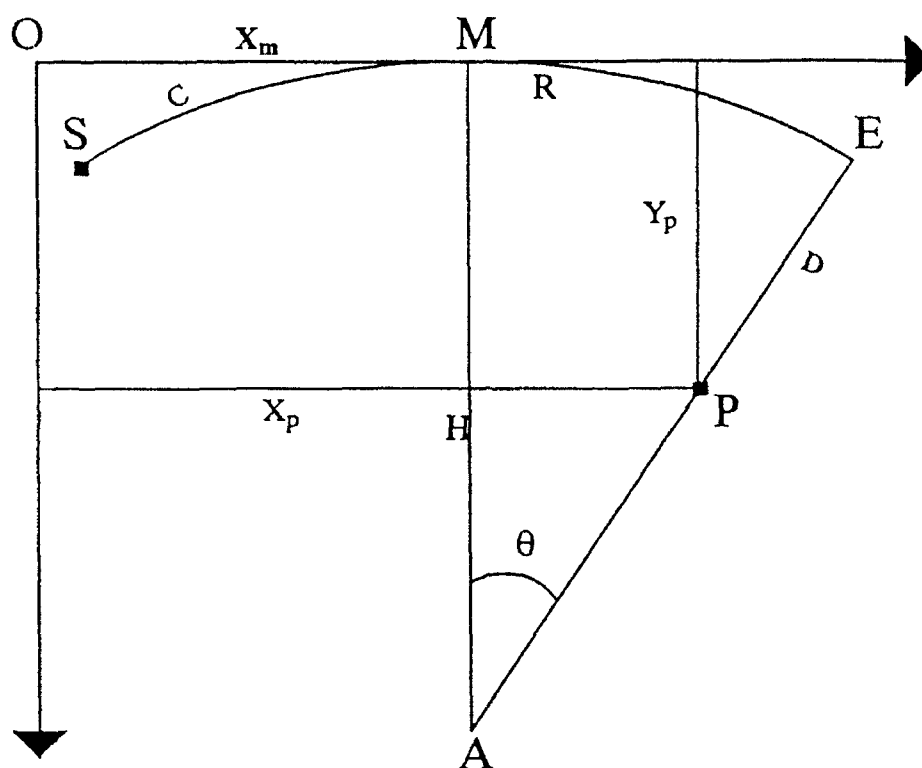


Figure 22: Graphic representation of earth curvature algorithm.

The user provides (R, D) of point P and the algorithm returns (X_p , Y_p).

P = subsurface position of some point within the user's model

E = point on surface directly above point P

S = origin for user's range/depth coordinate system

R = arc length from S to E (user input -- **range**)

D = radial distance from E to P (user input -- **depth**)

O = origin of Cartesian coordinate system

M = range at which the true Cartesian coordinate system is tangential to the curved earth

A = center of the earth

H = radius of the earth

C = arc distance from S to M

X_m = distance from O to M (= C)

$$\theta = (R - C) / H$$

$$X_p = X_m + (H - D) * \sin \theta$$

$$Y_p = H - (H - D) * \cos \theta$$

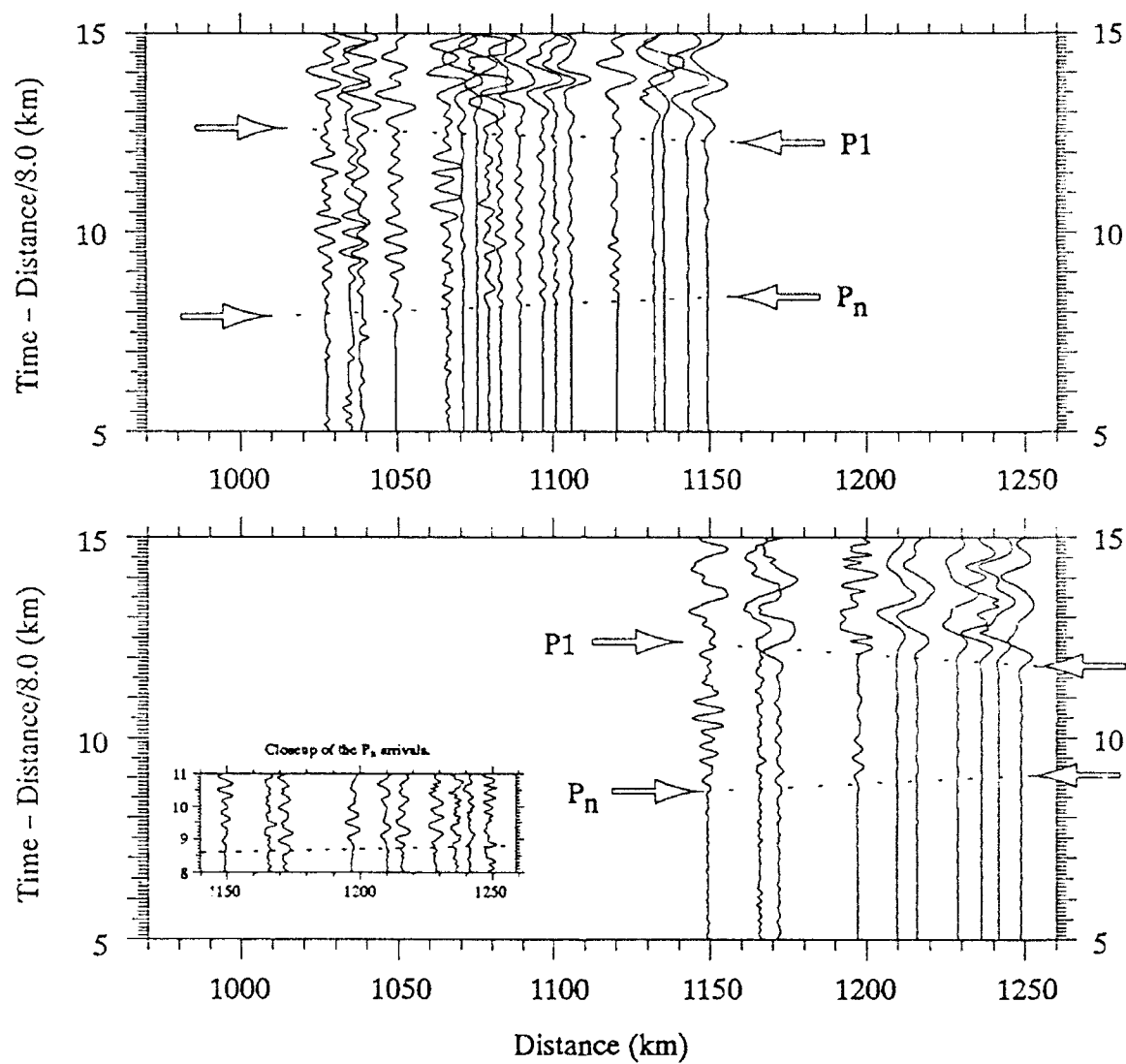


Figure 23: Seismic sections from NTS2 and NTS4 with phase arrivals labeled.

The top section is from shotpoints NTS1 and NTS2 and the bottom section is from NTS4. The inset shows a closeup of the P_n arrivals from NTS4.

about 10 sec are converging within the aperture of this work (1000 km to 1200 km). This is due partly to the nature of the synthetic model (several thin layers at depth) but the observed sections indicate similar multiple arrivals. Further analysis of these tightly clustered phases will have to wait for additional traces to be added to this survey in order to increase the aperture and make phase correlations easier. It should be noted however that in the observed sections, this packet of energy and the P_n arrivals arrive significantly later (~ 2 sec) than predicted by the 1D models. In addition, the P1 arrival does not appear to be as continuous across both sections as the P_n arrival. A significant delay in the P1 arrival is apparent between offsets of $R = 1050$ and $R = 1150$.

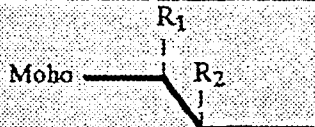
Initial Model

The initial model generated for this survey was derived from several sources. Crustal models were chosen from surveys within each of the separate geologic provinces that exist between NTS and the eastern extremes of the seismic array (Basin and Range, Colorado Plateau, Rio Grande Rift, and Great Plains) and an upper mantle model was drawn from regional studies in the western and central U.S. The combined model consisted of three crustal layers and several mantle layers extending to a depth of about 200 km.

Table 1 summarizes the various iterations used to model the P_n arrival. The best fit to the data is obtained with an "abrupt," 50-km wide transition zone between rift and cratonic crust extending from $R = 1150$ km to $R = 1200$ km. The crust thickens from 32 km to 51 km yielding an apparent dip along the Moho of approximately 21° . This centers the transition directly under the Pecos River. Bringing the transition closer to the rift (farther west) caused the modeled phases to arrive as much as 1 second later than the observed phases. Similarly, moving the transition to the east caused the modeled rays to arrive up to 1 sec too early. Analysis of a gravity profile along the trace of this seismic

line shows a large gravity gradient in eastern New Mexico which correlates with the general location of the crustal transition derived from this seismic study.

Table 1: Description of model iterations on the Moho transition within the study area. The highlighted box represents the best fit.

			
R ₁	R ₂	Description	Results
1050	1200	Broad transition beginning under the Sacramentos and extending to eastern banks of Pecos River.	Arrivals up to R=1150 km are very good. East of R=1150, arrivals are late, especially between R=1175 and R=1225 (>0.5 sec late, up to 1.2 sec late).
1050	1100	Extreme case with abrupt transition to cratonic crust under Sacramento Mountains.	Western arrivals OK. Model travel times begin to arrive too late by R=1120. By R=1200, predicted arrival is ~1 sec late.
1100	1150	Abrupt transition beginning at eastern end of Capitan Intrusion and ending 25 km west of Pecos River.	All arrivals east of R=1190 are about 1/2 sec late.
1150	1200	Abrupt transition centered on the Pecos River and extending approx. 25 km to either side.	Good fit across all P _n arrivals. Arrivals between 1100 and 1150 are very slightly early (0.1 - 0.15 sec).
1250	1260	Extreme case where no seismic energy reaches the transition.	Most arrivals from R=1100 km eastward are too early (0.1 - 1.0 sec).

Fewer constraints were available for the deeper parts of the model. As a first guess, the Burdick and Helmberger (1978) T7 model was used across this entire model beneath 65 km. The resultant P1 arrivals were about 1 sec early across most of the section and over 2 sec early in the region of R = 1100 km. However, by lowering the velocity in each of the layers under 65 km depth by only 0.06 km/sec, it was possible to get a reasonable fit across most of the section. The only mis-

match is in the region of the apparent delay in the observed P1 arrival time around $R = 1100$ km. On closer inspection, a very weak arrival can be detected across this entire region which is continuous with the larger arrival across the rest of the section. Since the data in each trace is normalized to a fixed amplitude height, a stronger arrival just behind the first P1 arrival dominates the signal in that time window. Therefore, the phase match for P1 is consistent across the entire section.

The exact source of the large secondary arrival in the P1 window is impossible to determine with this small data set. However, one possibility is energy that initially entered the bottom of the Colorado Plateau upper mantle but was then refracted by the large velocity variation in the upper mantle between the Plateau and the rift eventually reached the surface within the rift. It was possible to get some arrivals to do this through the model and they did have the proper arrival times, but the solution was very unconstrained and non-unique.

Figure 24a is a drawing of the final model derived from this work. The figure was drawn as a "flat earth," i.e. without the earth curvature approximations discussed above. Figure 24b shows all the rays which were used to construct the final model. Since the data had to be divided into 2 separate sections, the modeling was also divided. The solid rays are those that originated at shotpoint NTS1/NTS2 and the dashed rays are those that originated at NTS4. Figure 25 shows the NTS2 and NTS4 seismic sections plotted side-by-side and overlaid by the modeled arrival branches and Figure 26 uses velocity vs. depth profiles to show the differences between this model within the Rio Grande Rift and Burdick and Helmberger's (1978) model T7.

CONCLUSIONS

A number of conclusions can be drawn from the unreversed data presented here. First, the location of the crustal transition between the Rio Grande Rift and the Great Plains is about 50 km or more farther east than any surface features attributed to the rift (Figure 27). This indicates that the

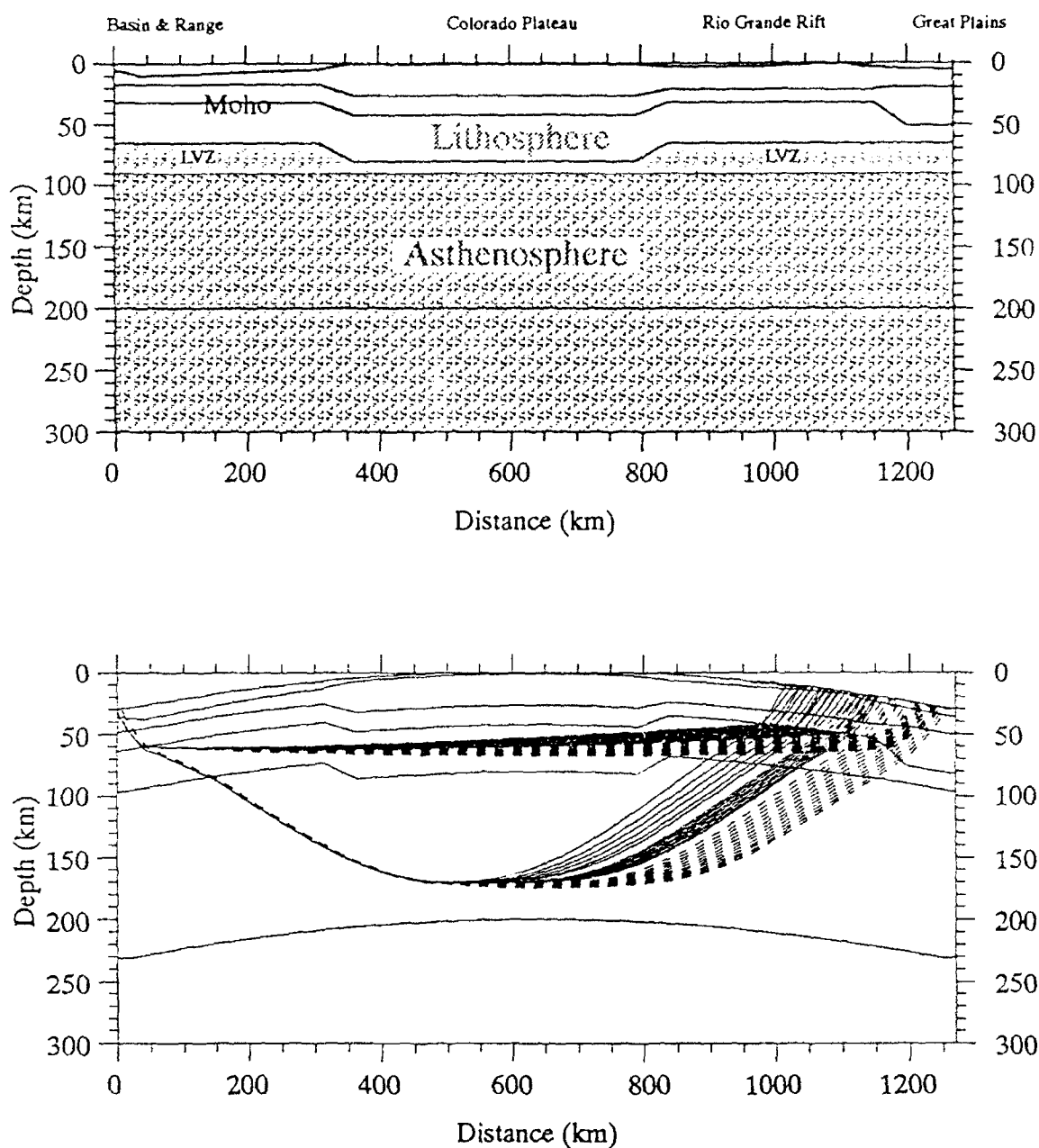


Figure 24: A) A plot of the final model from this work and B) the modeled raysets.

The structure of the final model beneath the horizontal line at 90 km in A) matches the structure of Burdick and Helmberger (1978).

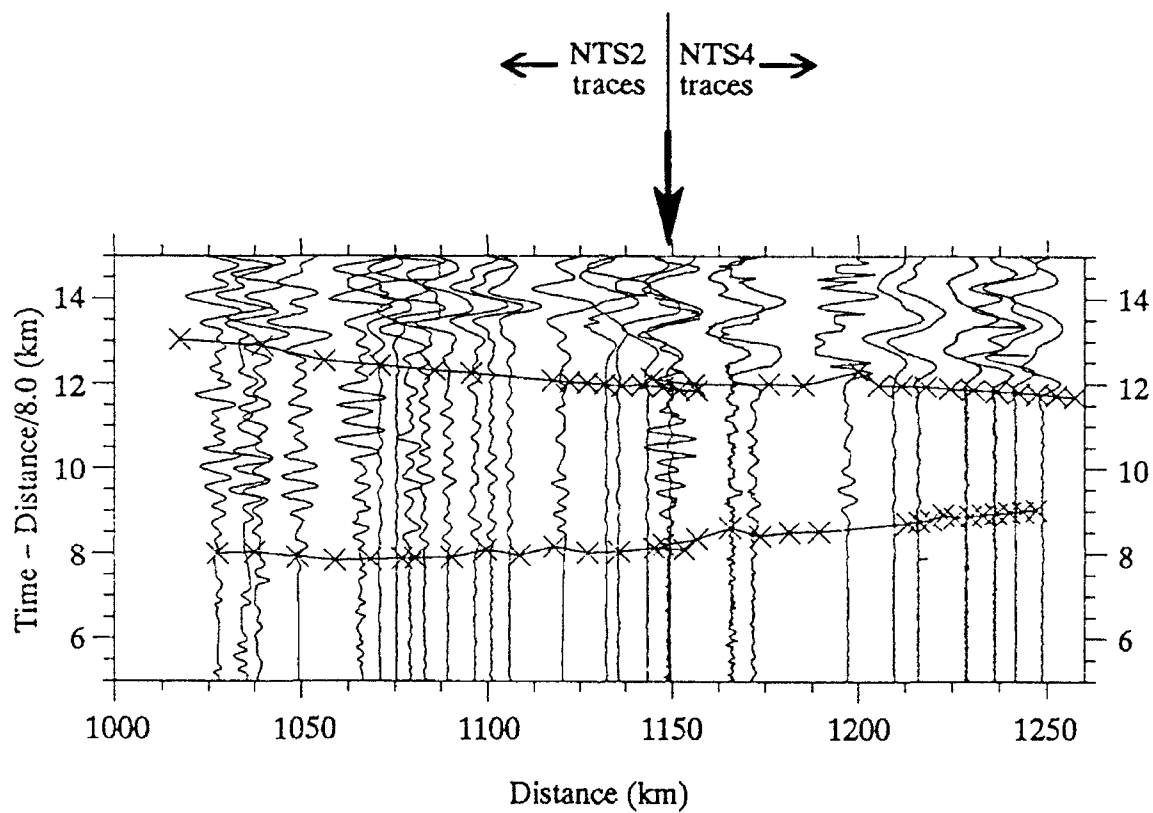


Figure 25: NTS1/NTS2 and NTS4 seismic section overlaid by modeled arrival branches.

The station at 1149 km was occupied for both shots. Data to its left is from NTS1/NTS2 and the rest is from NTS4.

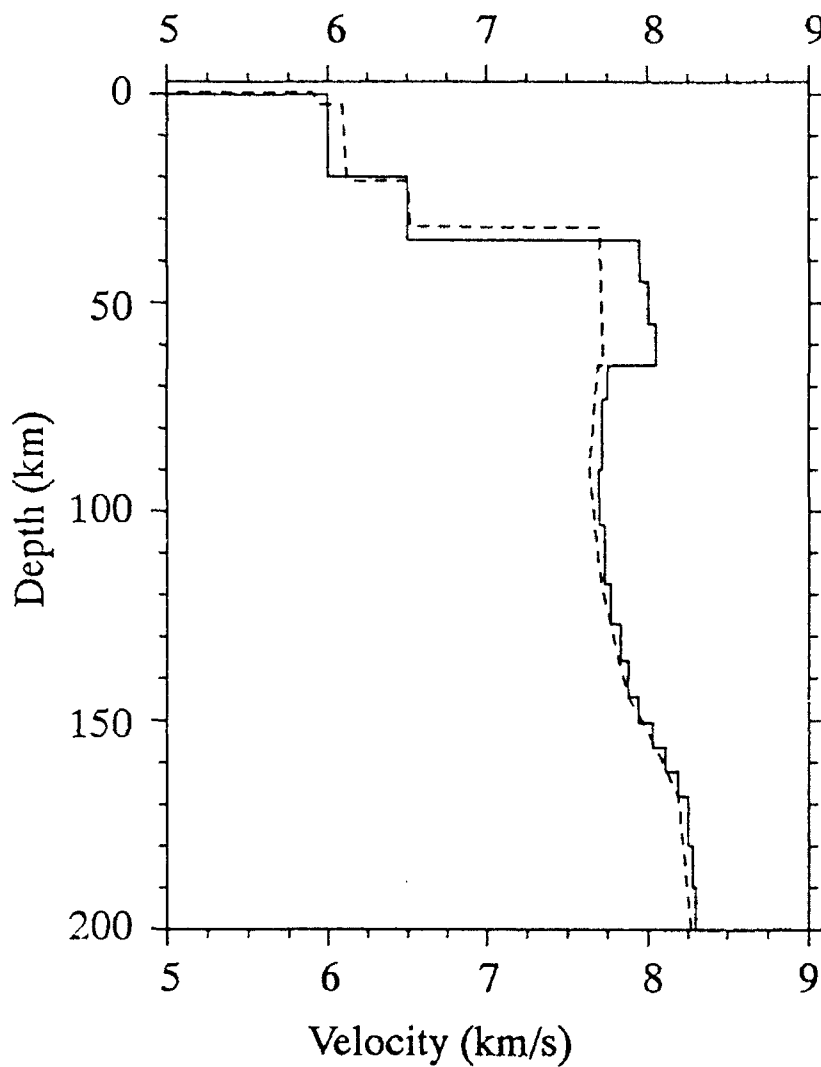


Figure 26: Velocity/Depth profiles within the Rio Grande Rift from the final model presented here and the Burdick and Helmberger (1978) model T7.

The solid line represents the T7 model and the dashed line is the model from this study. The profile was taken at $R = 1000$ km.

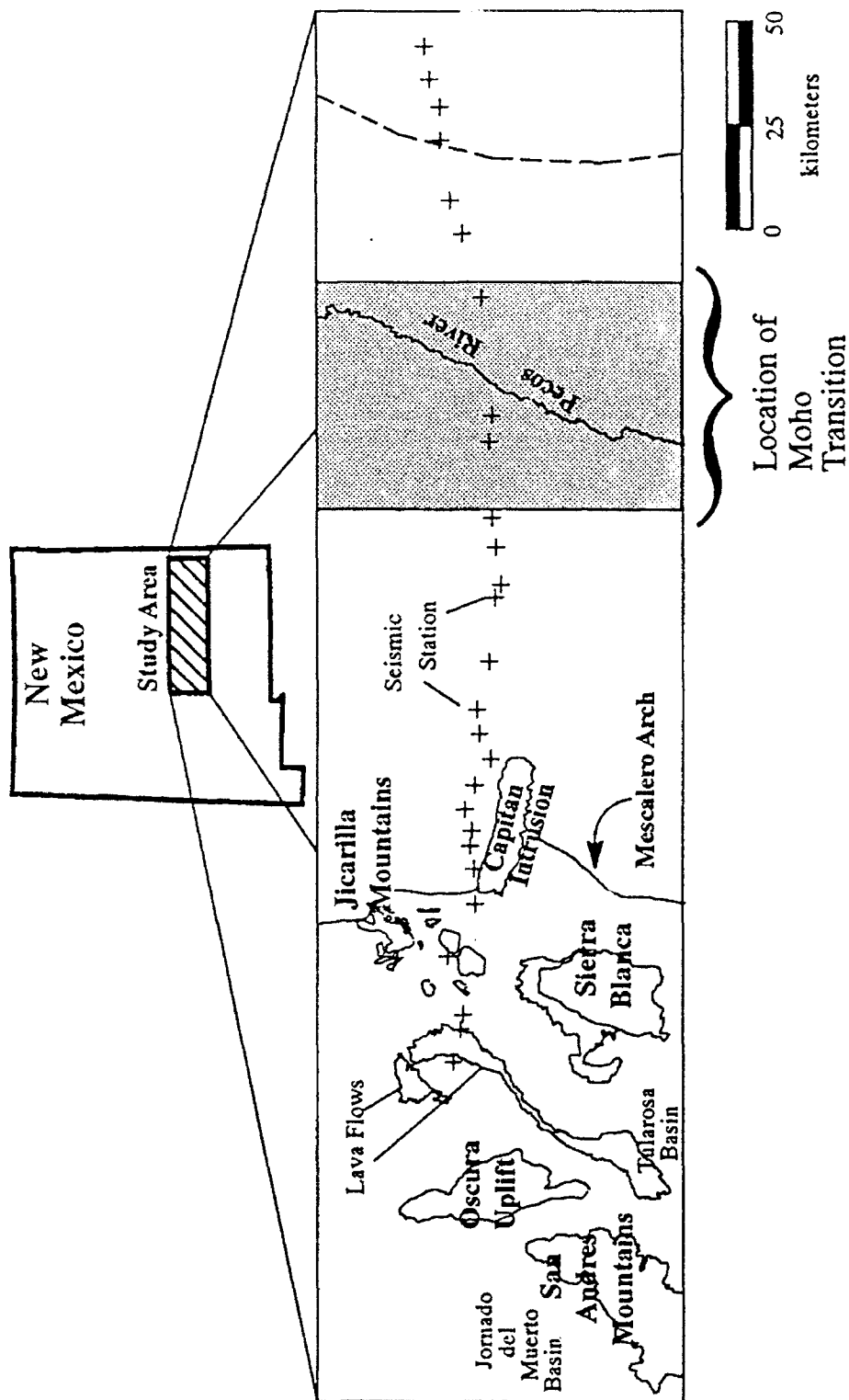


Figure 24: Map view of the location of the Moho transition zone between the Rio Grande Rift and the Great Plains as determined from this study.

The small discrepancy between the width of the transition zone and the length of the scale bar is caused by the slight off-line location of the shotpoints.

crustal thinning and associated mantle upwarp within the rift have undercut the westernmost Great Plains Province. It further confirms that the Tularosa basin is well within, and a product of, the Rio Grande Rift.

By comparing the synthetic sections generated from the 1D model of Burdick and Helmberger with the observed sections it is clear that the recorded energy in the study area traveled through significantly slower material than that predicted by the T7 model. Furthermore, the rift crust in the final model of this work is actually thinner and faster than that in the Burdick and Helmberger model (Figure 26). Therefore, the compressional velocities within the upper mantle and/or asthenospheric structure of the modeled area must be slower than the respective T7 structures. Unfortunately, the resolution of this survey is not sufficient to identify the exact location of the low velocity region. The anomaly can be accounted for with a 0.06 km/s adjustment to the T7 structures across the entire modeled area. This results in a less than 1% drop in velocity across the lithosphere/asthenosphere transition. However, the anomalously high surface heat flow and voluminous volcanics within the rift suggests that the low velocity anomaly may be isolated under the rift and would therefore represent more than just a 0.06 km/s velocity drop. Teleseismic investigations of the rift have indicated a depth to the low velocity zone of about 70 km under the north central part of the rift with an 8% velocity reduction. Burdick and Helmberger (1978) place the interface at a depth of 65 km for an average of the western U.S. with a velocity drop of 3.7%. Even using the upper mantle velocities from Burdick and Helmberger (1978), a velocity drop of 8% in the upper asthenosphere beneath the rift would result in velocities (~ 7.4 km/s) that are intuitively too low for that depth and would not match the refraction data presented here. The investigators who conducted the teleseismic study acknowledge that the 8% velocity reduction is extremely large but indicate that such a value is necessary to produce the large teleseismic delays they observed. The discrepancy between the teleseismic

results and refraction results may be explained by the different locations of the two profiles or the different paths that the seismic energy traveled before reaching the respective stations.

Preliminary Results from the Refraction Profile Extending Westward from the Minor Uncle Conventional Explosion at White Sands Missile Range

As part of our ongoing investigation of crustal structure between the White Sands Missile Range (WSMR) and the Nevada Test Site (NTS), UTEP deployed a seismic array in June, 1993, to record the Minor Uncle conventional surface explosion at WSMR. Three recording crews deployed a total of 68 stations at 1 mile intervals along US Highway 60 beginning west of Socorro, NM, and ending several miles west of Datil, NM (Figure 28). Each station consisted of a 1 Hz, vertical component, Mark Products L-4 seismometer and a USGS Seismic Cassette Recorder (SCR). These SCR units are automatic gain ranging, analog tape recorders built by the USGS. We used these older units because of the scheduling difficulties associated with the newer Seismic Group Recorders (SGRs) or the PASSCAL Reftek instruments. Our previous experiences with the SCRs have convinced us of their high reliability and excellent recording quality. The only limitation of the SCRs, a narrow recording window, was handled by maintaining good communications between the recording crews and the personnel at WSMR. In addition to the 68 SCRs, five digital Reftek recorders with three-component seismometers were deployed at widely spaced intervals along the line. These modern instruments were deployed primarily for us to acquire more experience with them and to compare their recording characteristics with those of the SCRs.

The Minor Uncle experiment went off as scheduled and 66 SCRs and all five Refteks recorded a strong signal. The resultant record section (Figure 29) is extremely sharp and shows a number of prominent arrivals. The PmP phase marked on the section represents the wide-angle reflections off of the crust/mantle transition and is a strong indicator of overall crustal structure. The approximately 7 sec arrival time of this phase at about 100 km compares well with much lower resolution surveys conducted just to the south of this profile. At the farthest offsets, it appears that the PmP signal is merging with P_n , the refracted arrival from the upper mantle. The most remarkable

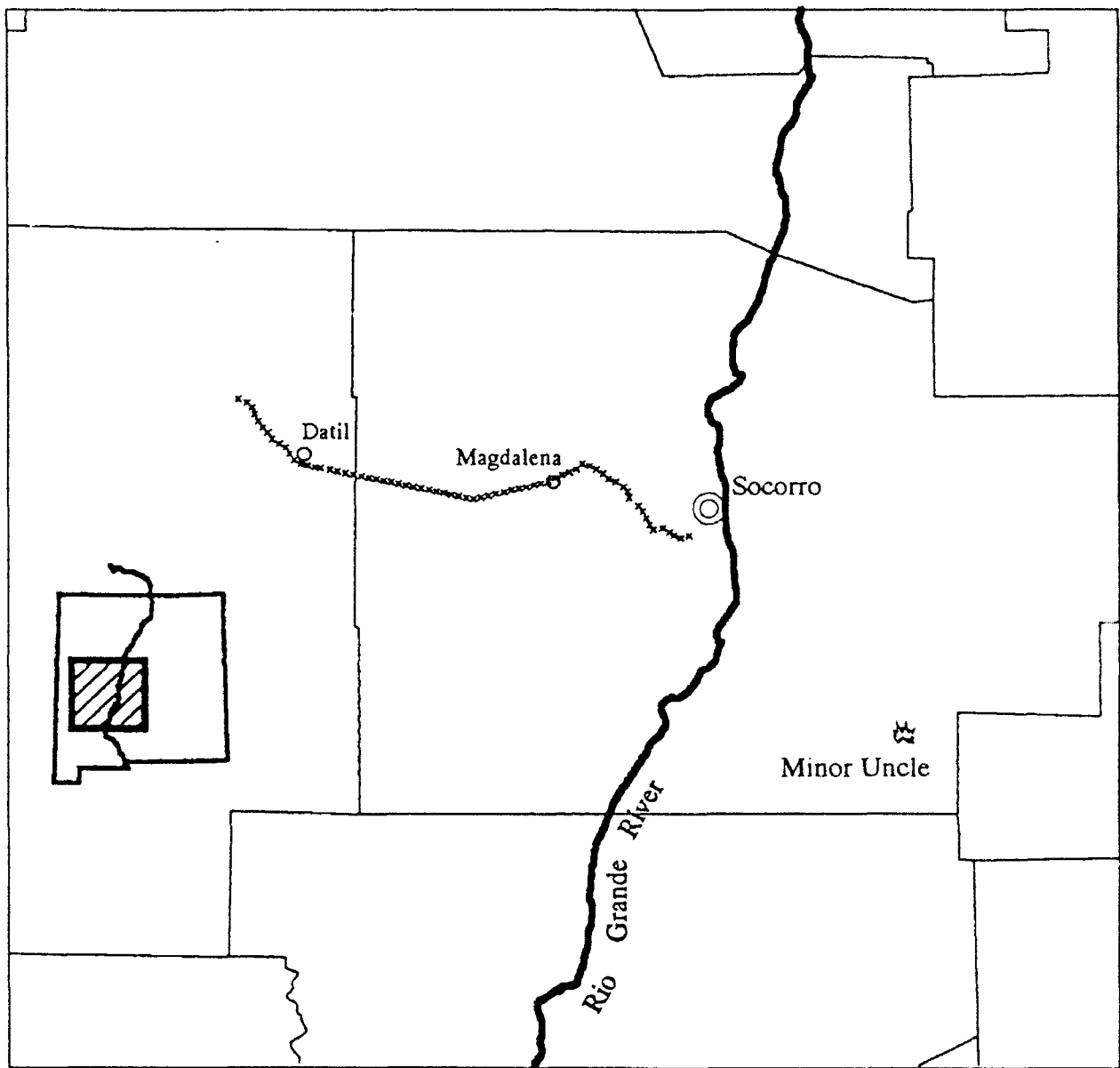


Figure 28: Basemap showing the location of the Minor Uncle conventional surface explosion and the seismic stations deployed by UTEP.

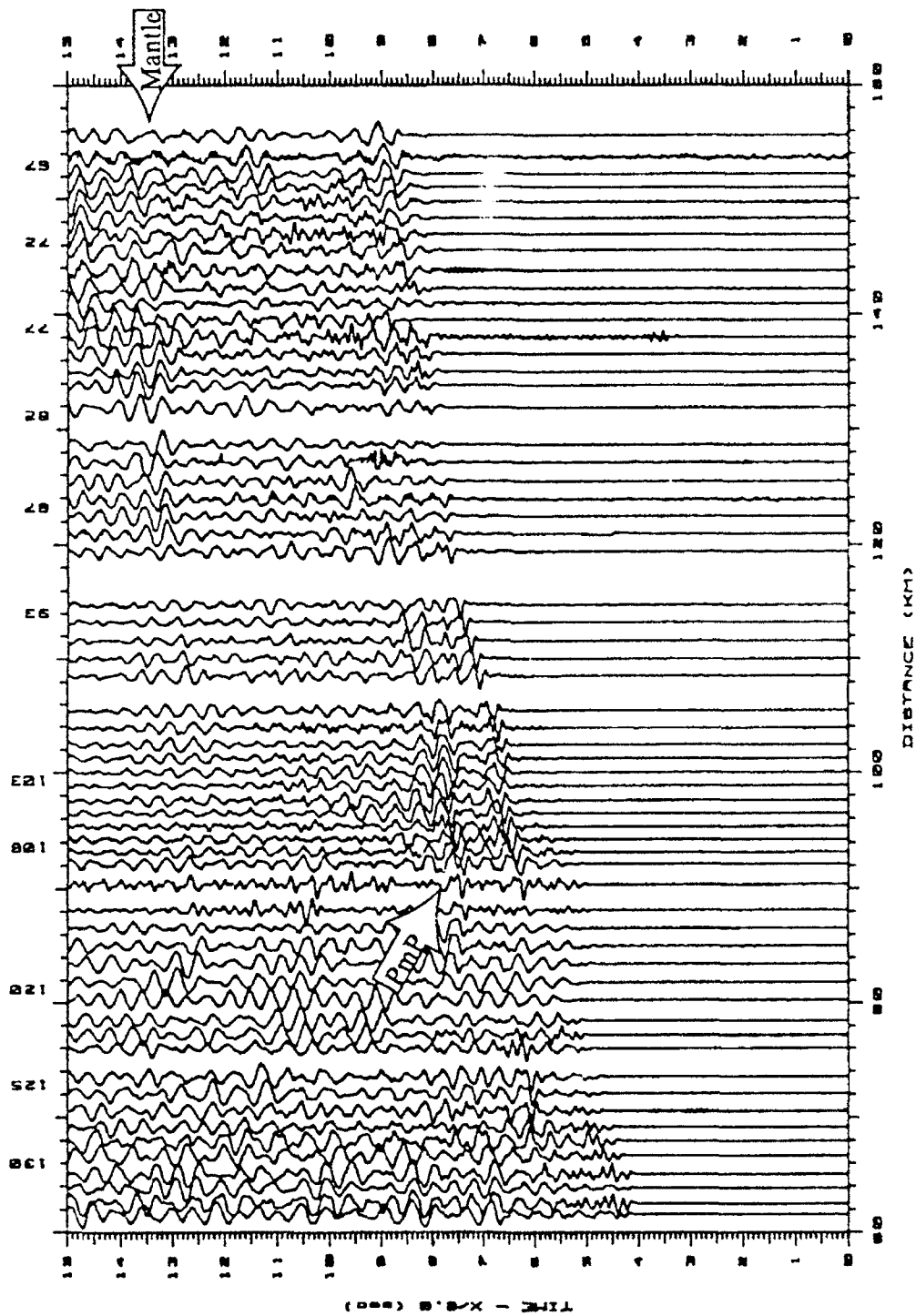


Figure 29: Seismic section generated from the data gathered during the Minor Uncles experiment at WSMR.

Arrows indicate the locations of the PmP and upper mantle reflection phases.

arrival on this section is the late arrival that crosses the western half of the section at about 13 seconds. This appears to be a reflection from within the upper mantle. Work is in progress to fully interpret these data and to evaluate their implications for the NTS-WSMR lithospheric transect.